Mechanisms of Electrospray Ionization of Singly and Multiply Charged Salt Clusters

ARTICLE *in* ANALYTICA CHIMICA ACTA · FEBRUARY 2000

Impact Factor: 4.51 · DOI: 10.1016/S0003-2670(99)00596-6

ELSEVIER

Analytica Chimica Acta 406 (2000) 67–91

ANALYTICA CHIMICA ACTA

www.elsevier.com/locate/aca

Mechanisms of electrospray ionization of singly and multiply charged salt clusters

M. Gamero-Castaño, J. Fernández de la Mora *

Department of Mechanical Engineering, Yale University, New Haven, CT 06520-8286, USA

Received 16 October 1998; accepted 15 April 1999

Abstract

Electrosprays of solutions of tetraheptyl ammonium bromide (A^+B^-) in formamide and propanol are investigated with a differential mobility analyzer (DMA) and a particle size magnifier (PSM) detector able to count single ions and to infer their charge state. The DMA can analyze all the charged species present, covering a vast range of masses and charge states, from $(A^+)_z(A^+B^-)_n$ clusters ($z = 1, 2, 3\ldots$; $n = 0, 1, 2, \ldots, 18, \ldots$), up to highly charged salt nanoparticles with diameters of tens of nanometers. Each charge state z appears only in a limited range of aggregation n, with $n_{\max}(z-1) \sim n_{\min}(z)$, which leads to a regular pattern of ordered modulations in the mobility spectra of the neutralized clusters (z reduced to 1). Coulomb explosions of the electrosprayed drops can be suppressed at will in solvents with electrical conductivities K higher than 1 S/m, as confirmed independently via energy analysis of the spray drops in a vacuum. The mobility spectra then change drastically, showing only singly charged clusters with $n = 0, 1, \ldots, 5$ (evidently field-evaporated) and large residues, with no traces of doubly or triply charged clusters in between. Coulomb explosions are therefore, responsible for the formation of all multiply charged clusters of intermediate sizes, covering the vast range from $(A^+)_2(A^+B^-)_4$ up to relatively large nanoparticles. But ion evaporation determines the charge state of all these residues. The resulting curves $n_{\max}(z)$ and $n_{\min}(z)$ hence carry key quantitative information on the kinetics of ion evaporation. This includes the dependence of the solvation energy $\Delta(R, z)$ on drop radius R and charge, which is also modelled theoretically in the Appendix A.

Keywords: Electrospray; Differential mobility analyzer; Particle size magnifier; Ion evaporation; Charged residue

1. Introduction

Electrospray ionization (ESI) has a well known ability to produce multiply charged ions [1–3], whose charge ez may be readily determined mass spectrometrically. z has hence been investigated over a wide range of ion structures and masses m [4,5], and the observed dependence of z on m has been used frequently to make inferences on the structure of the ion as well as on the ionization mechanism.

ESI also has a remarkable ability to produce ion clusters containing one or several neutral species attached to an anion or a cation. This phenomenon of 'fractional charging' [6,7] has been examined much less extensively than multiple charging. But a number of related articles have appeared and have provided additional clues on the nature of the ionization mechanism. The pioneering work of Meng and Fenn [7] constitutes still the most systematic study available on

* Corresponding author. Tel.: +1-203-4324347; fax: +1-203-4327654.
E-mail address: delamora@torus.eng.yale.edu (J. Fernández de la Mora).

0003-2670/00/$ – see front matter
PII: S0003-2670(99)00596-6

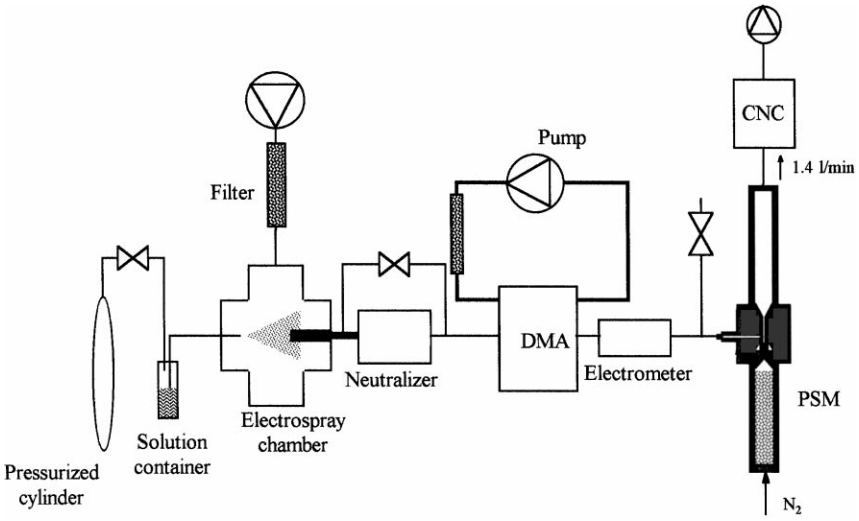

Fig. 1. Sketch of the experimental arrangement.

the effect of various physical and chemical variables on electrospray production of cluster ions. They observed clusters with up to 24 molecules of arginine ($m \sim 174$) attached to up to four protons. By relating their mass spectrometric observations to changes controllably induced in the solution, they argued that most of what was seen could be explained in terms of the ion evaporation model (IEM) of Iribarne and Thomson [8–11]. In contrast, most subsequent ESI cluster formation studies [12–19] have been interpreted in terms of some variant of Dole's charged residue mechanism. The work of Kebarle and his colleagues [20] is also most relevant in this respect.

The present study on cluster production in electrosprays is also aimed at elucidating the ionization mechanism. With that purpose in mind, we have introduced several experimental innovations. First, the use of a differential mobility analyzer (DMA) of unusually high resolution [21–23], rather than a mass spectrometer, allows simultaneous observation of small clusters as well as large particle residues. Second, the particle size magnifier (PSM) detector used offers a formidable improvement in sensitivity over previous work, even for sub-nanometer species, and, furthermore, allows the determination of their charge state. In addition, we are able to suppress Coulomb fissions by use of highly conducting solutions, whose electrosprayed drops shed charge directly via ion-evaporation rather than by exploding. The driving force for Dole's ionization mechanism is hence eliminated, allowing the observation of the clusters formed purely by field evaporation, and enabling the determination of which part is played by each of these two ionization mechanisms.

2. Experimental

The experimental set up is shown in Fig. 1. Charged particles generated in an electrospray chamber and with a given electrical mobility, Z, were selected using a DMA of unusually high resolving power, [23]. Z is related to the charge, q, and the 'mobility diameter' of the particle, D, through the expression

$$Z = 0.4428 \frac{q(kT/m)^{1/2}}{p(D + d_0)^2} \quad (1)$$

which is a modified version of Millikan's formula for spheres in the free molecular regime [24–26]. p, T, m and k stand for the gas pressure, absolute temperature, molecular mass of the carrier gas and Boltzmann's constant. This expression accounts for the effect of the finite diameter of the molecules of the suspending gas, $d_0 = 0.53$ nm [24–26], and will be used in this work whenever mobility diameters are estimated. In order to compute the mobility of the clusters we calibrate

Table 1
Characteristics of the electrolytes sprayed

Solution	Solvent	Concentration (M)	Conductivity (S/m)
FOR1	Formamide	0.00535 THABr	0.123
FOR2	Formamide	0.189 THABr	0.235
FOR3	20% (v) water in formamide	0.080 THABr & 0.486 TEAOH	1.16
FOR4	Formamide	0.0090 THABr & 2.0 AcA	1.51
FOR5	Formamide	0.063 THABr & 1.3 AcA	1.14
PRP1	Propanol		2.43×10^{-4}

the abscissa of most of the spectra using the mobility of the cluster $A^+(A^+B^-)_2$ as a standard. Its absolute value in ambient air at 99 300 Pa and 25°C has been determined to be 0.663 cm^2/Vs with another DMA characterized previously [21].

The multiply charged ions and particles sampled from the electrospray chamber could be partially discharged by exposure to a radioactive source (Nuclespot Local Air Ionizer, model P-2042, 5 mCi, NRD, Grand Island, New York). The DMA then selected clusters and particle residues within a narrow mobility range, and introduced them into a PSM [27]. The PSM surrounds the ions with supersaturated vapors of dibutyl phthalate, whose saturation ratio S

$$S = \frac{p}{p_v(T)} \tag{2}$$

can be finely controlled (p is the partial pressure of dibutyl phthalate vapors, and $p_v(T)$ its equilibrium vapor pressure at temperature T). Beyond a critical supersaturation S^*, ions grow into large drops, each of which is counted optically with a condensation nucleus counter (CNC, model 3760, TSI, St. Paul, Minnesota; nominal detection size limit ~10 nm). The sensitivity of this PSM detector is several orders of magnitude higher than that of the electrometer commonly used as detector in our DMA.

As the critical value S^* at which a certain ion grows into a large drop depends on its size and charge, the PSM can be used to infer the charge state of the ions [28]. The PSM used in this work modifies the instrument developed by Okuyama et al. [27] and is the first CNC-type instrument able to detect sub-nanometer clusters [29,30].

Several solutions of tetraheptyl ammonium bromide (THABr) in formamide (from Sigma) and propanol (from J.T. Baker) were analyzed. The use of this relatively large organic salt was motivated by the simplicity of its ionic spectra, free from multiple states of solvation (see [9], for instance). Suppressing Coulomb explosions of the charged drops requires electrical conductivities of the order of 1 S/m [31], and hence highly polar solvents such as water and formamide. The later was chosen because its low volatility facilitates the stabilization of the Taylor cone at such high electrical conductivities and corresponding minuscule liquid flow rates. The concentrations and electrical conductivities of all solutions used are collected in Table 1.

3. Unraveling the mobility distributions

Figs. 2–4 show the CNC signal at various values of the supersaturation S in the PSM. All the runs are for solution FOR1, at constant liquid flow rate ($Q = 0.845$ nl/s), and without electrically discharging the aerosol. The abscissa values are given in units of inverse mobility (Vs/cm^2), as measured by the DMA, while the ordinate is in arbitrary units. Fig. 2 plots curves corresponding to supersaturations ranging from 0 to 243. For $S = 0$, only relatively large particles can be seen (the nominal detection limit of our CNC is 10 nm, though smaller multiply charged particles are probably detectable [28]), showing two modes centered at 2.3 and 2.8 Vs/cm^2. We can see that the curve for the residues with $Z^{-1} > 2.8$ Vs/cm^2 appears to be saturated at $S = 0$, implying that all particles in this mode have relatively large diameters. In contrast, the area below the curves corresponding to the most mobile residues increases continuously with S, and therefore, contains rather small particles. Both types of residues appear to have a continuous distribution of charge and size at the limited resolution of our DMA.

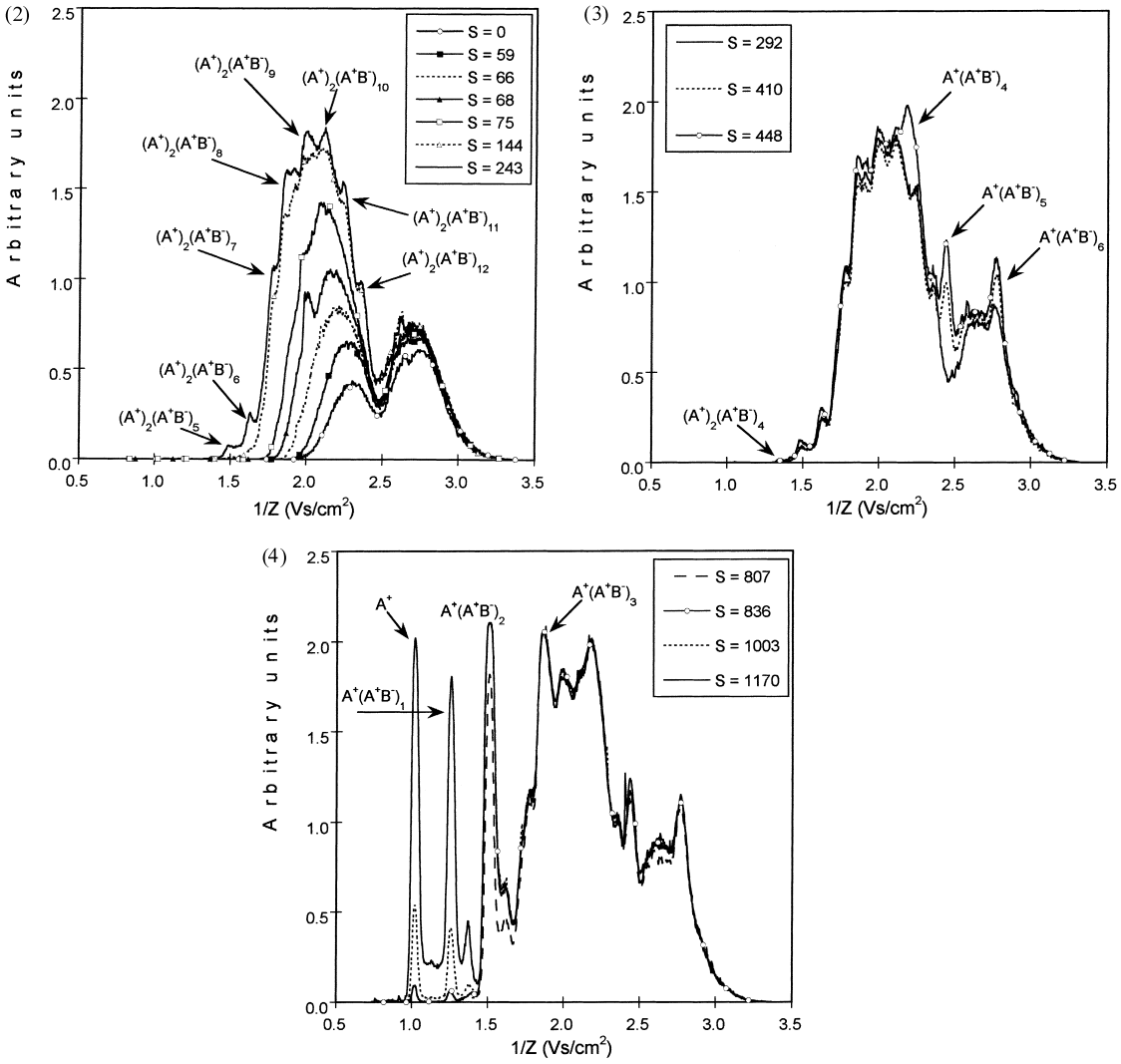

Figs. 2–4. CNC signal vs. inverse mobility at various PSM supersaturations for FOR1. Liquid flow rate $Q = 0.845$ nl/s.

Notice a narrow peak appearing at 2.0 Vs/cm^2 and $S = 68$, which is lost in the background at higher S. The appearance of new peaks may also be guessed at 1.9 and 1.7 Vs/cm^2 in the form of slight changes in the slope of the curve associated with $S = 75$. If S is further increased, a series of sharply defined peaks begins to emerge at $S = 144$ and becomes more evident at $S = 243$. We will see in Section 5.1 that they are doubly charged clusters with structure $(A^+)_2(A^+B^-)_n$ composed of n salt molecules A^+B^- with two tetraheptylammonium ions (A^+). In Fig. 3 we augment again the supersaturation. For $S = 292$ a new peak rises at 2.83 Vs/cm^2. We shall see that it is due to the singly charged cluster $A^+(A^+B^-)_6$. Two new singly charged clusters are detected in Fig. 3 at 2.46 and 2.19 Vs/cm^2 when S is raised up to 410 and 448, respectively. In Fig. 4 we collect four CNC curves obtained at still higher supersaturations. Four more singly charged clusters are observed at 1.88, 1.51, 1.28 and 1.04 Vs/cm^2.

The partial discharging of the residues leads to a better understanding of the aerosol, as shown in Fig. 5, $S = 292$. The doubly charged clusters may be seen more clearly than in Fig. 2, because the continuous background of highly charged residues shifts

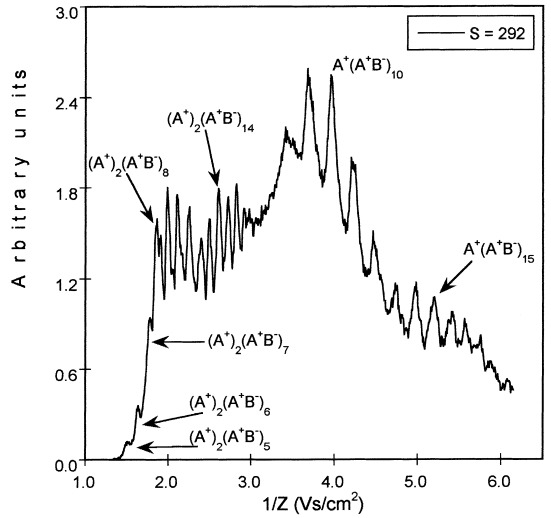

Fig. 5. CNC signal vs. inverse mobility for FOR1. Liquid flow rate $Q = 0.845$ nl/s, PSM supersaturation $S = 292$. The aerosol is slightly discharged.

to a zone of lower mobilities. A new series of peaks appears at lower mobilities, corresponding to initially multiply charged residues having lost all but one of their original charges. Fig. 6 is for the neutralized spray at different values of S. The degree of discharging in this case is higher than in Fig. 5, which leads to the disappearance of most of the doubly charged residues. Two features deserve especial attention: first, S^* increases as the mobility of the peak augments. Second, the new series of peaks resulting from neutralization of the spray extends continuously the original series of singly charged clusters. Note the presence of several new high mobility ions ($Z^{-1} = 0.88$, $1.18\,\mathrm{Vs/cm^2}$) formed in the neutralizer, and present even when the spray is turned off.

The peaks in Fig. 6 marked $A^+(A^+B^-)_5$ and $A^+(A^+B^-)_6$ are not as narrow as their companions. In particular, $A^+(A^+B^-)_5$ seems to be formed by a second ionic species at its low Z tail. Using a higher degree of neutralization and a larger DMA resolution one sees in Fig. 7 that the peaks marked as $A^+(A^+B^-)_5$ and $A^+(A^+B^-)_6$ in Fig. 6 contain actually four species: $A^+(A^+B^-)_5$, $A^+(A^+B^-)_{5bis}$, $A^+(A^+B^-)_6$ and $A^+(A^+B^-)_{6bis}$. It will become clear that $A^+(A^+B^-)_{5bis}$ is the cluster $(A^+)_2(A^+B^-)_4$ partially discharged by attachment of an unidentified neutralizing anion N^-. Therefore, $A^+(A^+B^-)_{5bis} = A^+(A^+B^-)_4(A^+N^-)$, and its slight mobility difference with $A^+(A^+B^-)_5$ is due to the fact that the neutralizing ion N^- is larger than the Br^- ion it substitutes. One can similarly infer that $A^+(A^+B^-)_{6bis} = A^+(A^+B^-)_5(A^+N^-)$. The possibility to distinguish the 'bis' peaks in the partially

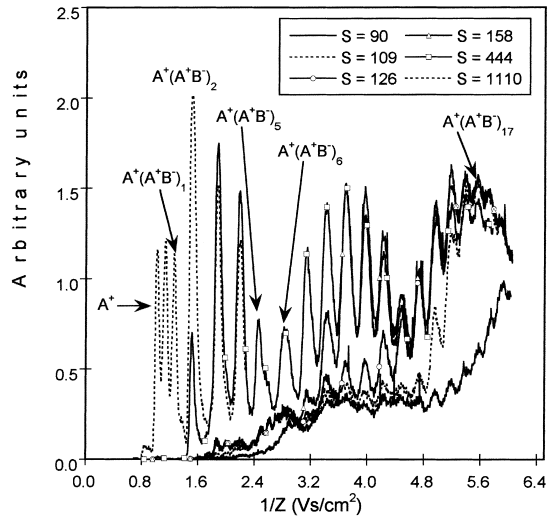

Fig. 6. CNC signal versus inverse mobility for a partially discharged FOR1 spray. Liquid flow rate $Q = 0.845$ nl/s. Each curve corresponds to a different PSM supersaturation.

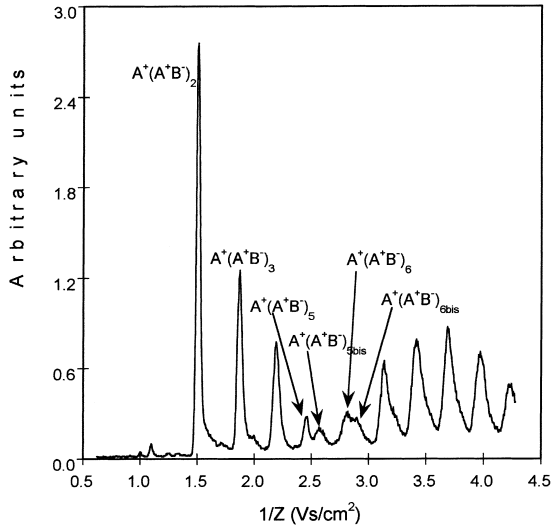

Fig. 7. CNC signal vs. inverse mobility for a partially discharged FOR1 spray. Liquid flow rate $Q = 0.845$ nl/s. A larger DMA resolution than that used in Fig. 6 is able to resolve the double structure of peaks $A^+(A^+B^-)_5$ and $A^+(A^+B^-)_6$.

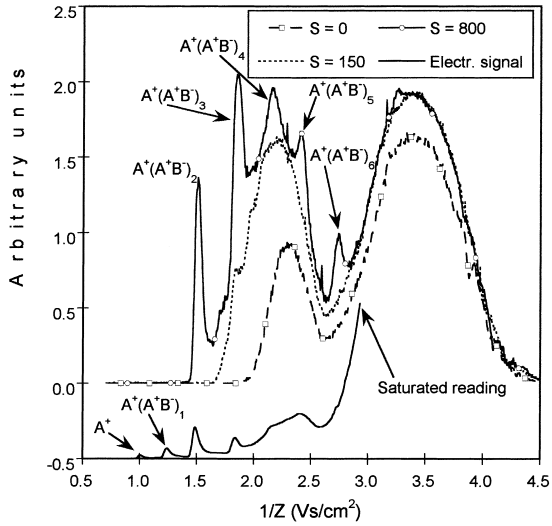

Fig. 8. CNC and electrometer signals vs. inverse mobility for FOR2. The CNC spectra are obtained at different values of the PSM supersaturation.

neutralized spectra will later be used as a marker for their doubly charged parents under conditions where the parents themselves are difficult to distinguish from the background.

Fig. 8 corresponds to a non-neutralized spray of solution FOR2. The sizes of the original drops are similar to those for the FOR1 experiments already described, but the ratios z/n of net charge over number of salt molecules are quite different for both solutions (see Table 2). Again, the residues can be divided into two regions. The most mobile group is centered at the same value of Z^{-1} as in the spray of FOR1. Although the least mobile mode has now a broader distribution of mobilities, as expected, the phenomenology observed is similar for both sprays.

Table 2
Electrospraying conditions for each of the sprays investigated[a]

Solution	Q (nl/s)	I (nA)	z/n	$\langle D\rangle$ (nm)	$\langle E\rangle$ (V/nm)
FOR1	0.845	182	0.42	151	0.61
FOR2	0.474	189	0.022	100	0.75
FOR3	0.0958	188	0.25	34	1.28
FOR3	0.176	256	0.19	32	1.16
FOR3	0.272	318	0.15	49	1.08
FOR3	0.465	416	0.12	58	0.99
FOR4	0.108	228	2.43	38	1.32
FOR4	0.225	329	1.68	42	1.16
FOR4	0.303	381	1.45	46	1.10
FOR4	0.434	457	1.21	53	1.03
FOR5	0.109	199	0.321	36	1.25
FOR5	0.284	322	0.187	50	1.07

[a] Q: liquid flow rate; I: spray current; z/n: average number of net charges over number of THABr molecules for the initial electrospray drop. $\langle D\rangle$ and $\langle E\rangle$ are the mean initial drop diameter and associated surface electric field (Eqs. (16), (17)).

The rather different set of experimental results reported in Figs. 9–11 is meant to show the radical

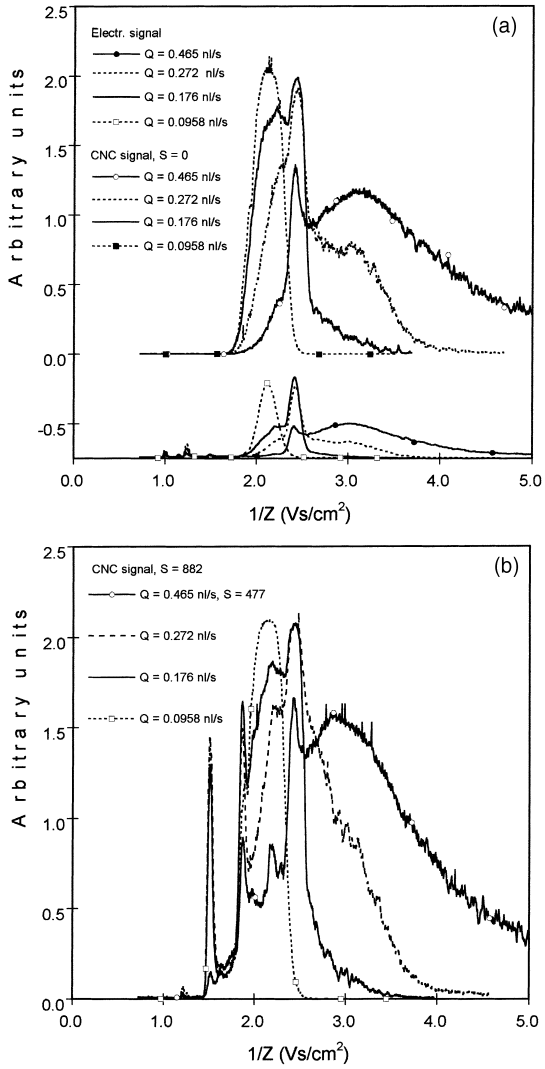

Fig. 9. Mobility spectra for FOR3, at various liquid flow rates (0.465 nl/s, 0.272 nl/s, 0.176 nl/s and 0.0958 nl/s, respectively). The bottom of (a) shows the electrometer signal, while the CNC signal above is for $S=0$. (b) shows the CNC signal for $S=882$ at all but the largest flow rate (for which $S=447$).

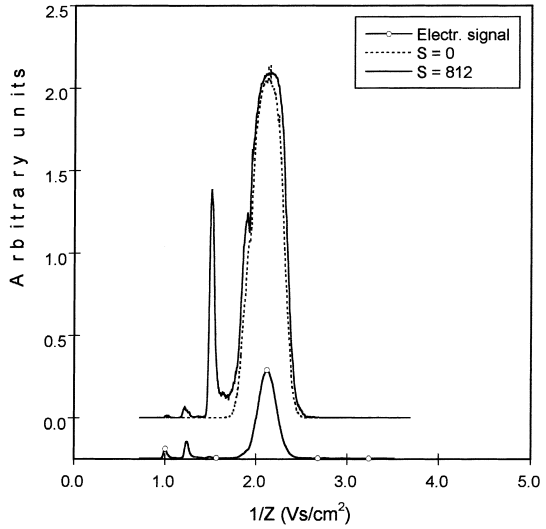

Fig. 10. Comparison of two of the curves of Fig. 9 at the smallest liquid flow rate (0.0958 nl/s). The main peak is clearly composed of large residues (activated at $S = 0$) and singly charged clusters, with unmeasurable contributions from small multiply charged clusters.

structure changes arising in the mobility spectra as one varies the flow rate of electrosprayed liquid in highly conducting solutions. We shall later argue that this metamorphosis is due to the increase in the electric field on the drop surface, which leads to the onset of ion evaporation, and hence the suppression of Coulomb explosions needed to support Dole's ionization mechanism. The figures correspond to solution FOR3, a mix of water (20% in volume) in formamide, where addition of tetraethylammonium hydroxide (TEAOH) increases the electrical conductivity to a value of 1.16 S/m. Fig. 9a shows the evolution of the mobility spectra as a function of liquid flow rate, as measured by the electrometer (lower traces) and the PSM at $S = 0$. Both detectors show how the broad peak centered at 3 Vs/cm^2 and the narrow peak at 2.4 Vs/cm^2 shrink steadily and disappear completely at the smallest flow rate included. Fig. 9b depicts the same process at higher PSM supersaturations, where $S = 812$ for all curves except for the one labeled with open circles (for which $S = 447$). This last curve exhibits a variety of sharp ionic peaks in the interval between 1.5 and 2.5 Vs/cm^2, some of which can be identified as doubly charged clusters. These clusters disappear also entirely at the minimum flow rate. This point is better seen in Fig. 10, where the difference between the CNC signal at $S = 0$ and $S = 812$ is negligible everywhere except for the presence of a few singly charged clusters. The disappearance of the doubly charged ions at the minimum flow rate is confirmed further in the mobility spectra included in Fig. 11. They correspond to a series of experiments with partially neutralized sprays at the same flow rates investigated in Fig. 9. For the two highest flow rates, at least ten singly charged clusters are observed (the smallest ones are not detected due to the limited supersaturation used in the PSM), with the same mobilities as those in Fig. 5. The situation changes for the lowest flow rate, when only the five smallest clusters are present in the spray. In conclusion, the reduction of the flow rate leads to the disappearance of the broad and the sharp peaks otherwise present at low mobilities, as well as to the elimination of the small multiply charged clusters. All that is left are a few singly charged clusters, and a sharp continuous peak centered at 2.2 Vs/cm^2. We shall argue in Section 5.5 that the disappearance of the high as well as the low mobility peaks is due to the suppression of Coulomb explosions.

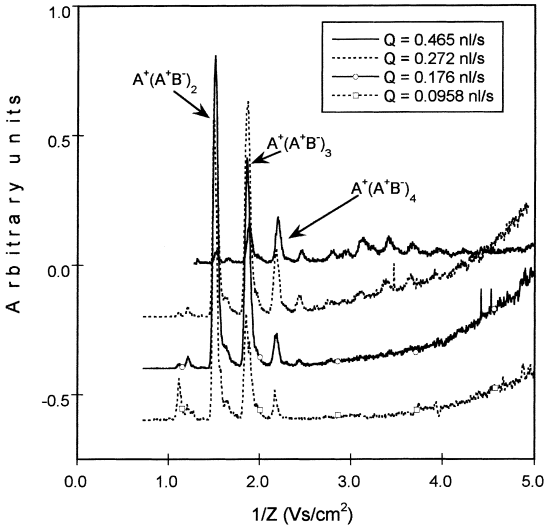

Fig. 11. CNC signal vs. inverse mobility for partially discharged FOR3 sprays, at various liquid flow rates (0.465, 0.272, 0.176 and 0.0958 nl/s).

As a confirmation of the drastic change of behavior arising at sufficiently small flow rates and high liquid conductivities, we have repeated these tests with the volatile salt ammonium acetate instead of the

Table 3
Characteristics of the clusters observed. $1/Z$ values are referred to atmospheric air at 99300 Pa and 25°C[a]

	$n+z$	$1/Z$ (Vs/cm^2)	Diameter (nm)	E (V/nm)	q/q_R (D)
Cluster ($z=1$)					
A^+	1	1.04	0.944	6.45	0.863
$A^+(A^+B^-)_1$	2	1.28	1.10	4.74	0.685
$A^+(A^+B^-)_2$	3	1.51	1.25	3.71	0.570
$A^+(A^+B^-)_3$	4	1.88	1.45	2.73	0.454
$A^+(A^+B^-)_4$	5	2.19	1.61	2.22	0.388
$A^+(A^+B^-)_5$	6	2.46	1.74	1.91	0.346
$A^+(A^+B^-)_{5bis}$[b]	6	2.59	1.80	1.78	0.329
$A^+(A^+B^-)_6$	7	2.83	1.90	1.59	0.303
$A^+(A^+B^-)_{6bis}$[b]	7	2.87	1.92	1.56	0.298
$A^+(A^+B^-)_7$[b]	8	3.14	2.03	1.39	0.274
$A^+(A^+B^-)_8$[b]	9	3.43	2.15	1.25	0.252
$A^+(A^+B^-)_9$[b]	10	3.70	2.25	1.14	0.235
$A^+(A^+B^-)_{10}$[b]	11	3.98	2.35	1.04	0.220
$A^+(A^+B^-)_{11}$[b]	12	4.24	2.45	0.962	0.207
$A^+(A^+B^-)_{12}$[b]	13	4.50	2.54	0.895	0.196
$A^+(A^+B^-)_{13}$[b]	14	4.74	2.62	0.841	0.187
$A^+(A^+B^-)_{14}$[b]	15	4.99	2.70	0.789	0.179
$A^+(A^+B^-)_{15}$[b]	16	5.21	2.77	0.751	0.172
$A^+(A^+B^-)_{16}$[b]	17	5.41	2.83	0.718	0.166
$A^+(A^+B^-)_{17}$[b]	18	5.59	2.89	0.691	0.162
$A^+(A^+B^-)_{18}$[b]	19	5.85??	2.97 ??		
Cluster ($z=2$)					
$(A^+)_2(A^+B^-)_4$	6	~1.38	1.87	3.28	0.618
$(A^+)_2(A^+B^-)_5$	7	1.53	2.00	2.88	0.561
$(A^+)_2(A^+B^-)_6$	8	1.64	2.08	2.65	0.527
$(A^+)_2(A^+B^-)_7$	9	1.80	2.21	2.36	0.483
$(A^+)_2(A^+B^-)_8$	10	1.87	2.26	2.25	0.466
$(A^+)_2(A^+B^-)_8$	10	1.91	2.30	2.18	0.455
$(A^+)_2(A^+B^-)_9$	11	2.01	2.36	2.06	0.436
$(A^+)_2(A^+B^-)_{10}$	12	2.13	2.45	1.92	0.413
$(A^+)_2(A^+B^-)_{11}$	13	2.26	2.54	1.78	0.391
$(A^+)_2(A^+B^-)_{12}$	14	2.40	2.64	1.66	0.371
$(A^+)_2(A^+B^-)_{13}$[b]	15	2.50	2.70	1.57	0.357
$(A^+)_2(A^+B^-)_{14}$[b]	16	2.62	2.78	1.49	0.342
$(A^+)_2(A^+B^-)_{15}$[b]	17	2.73	2.85	1.42	0.330
$(A^+)_2(A^+B^-)_{16}$[b]	18	2.84	2.91	1.36	0.319
$(A^+)_2(A^+B^-)_{17}$[b]	19	2.92	2.97	1.31	0.310
$(A^+)_2(A^+B^-)_{18}$[b]	20	2.99???	?		

[a] z is the net charge and n the number of neutral salt molecules. The cluster mobility diameter is based on the measured Z and Eq. (1). E is the corresponding surface electric field based on z and the cluster mobility diameter. The Rayleigh charge in q/q_R is based on the cluster mobility diameter and the surface tension of pure formamide.

[b] Implies that the cluster has been observed only after partial neutralization.

involatile TEAOH. This will clear the spectra from the residues associated to this hydroxide, which obscure partially the picture observed in Figs. 9–11. The cleanup will result not only from the disappearance of small clusters containing TEAOH, but also of the background of larger multiply charged nanoparticles. Solution FOR5 hence uses a mixture of tetraheptyl ammonium bromide and ammonium acetate (AcA) in formamide. Fig. 12 corresponds to this solution, with $Q = 0.284$ nl/s. The non-neutralized aerosol is described by the DMA's electrometer and CNC curves, while the neutralized spray is characterized

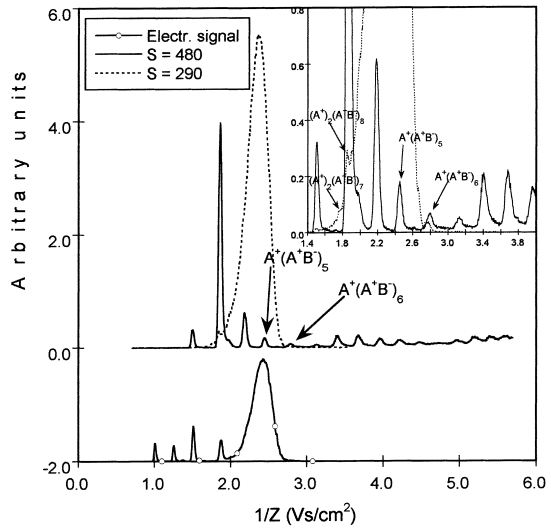

Fig. 12. CNC and electrometer signals vs. inverse mobility for FOR5. Liquid flow rate $Q = 0.284$ nl/s. Both original and partially discharged sprays are shown.

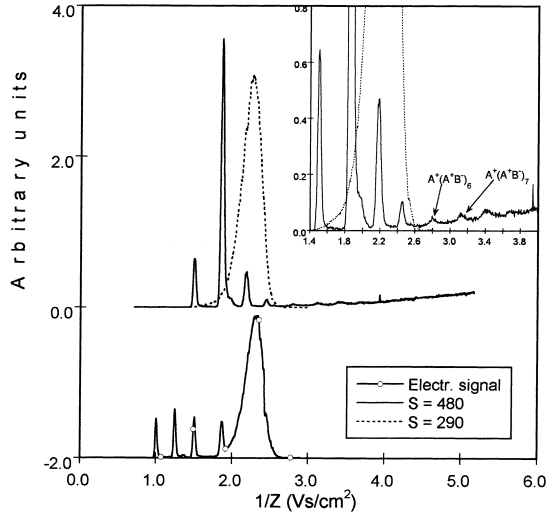

Fig. 13. CNC and electrometer signals vs. inverse mobility for FOR5. Liquid flow rate $Q = 0.109$ nl/s. Both original and partially discharged sprays are shown.

by the CNC curve. The mean diameter of the original drops is of some 50 nm, large enough (as we shall argue in Section 5.5) for the drops to undergo several Coulomb explosions. All the singly charged clusters listed in Table 3 are present in the neutralized spray, with the notable exception of $A^+(A^+B^-)_{5bis}$ and $A^+(A^+B^-)_{6bis}$. This is more clearly observed in the enlarged window shown in the right upper corner of Fig. 12: the signals due to $A^+(A^+B^-)_5$, $A^+(A^+B^-)_6$, $A^+(A^+B^-)_7$, $A^+(A^+B^-)_8 \ldots$ stand up strongly over the background, while the particles detected around 2.59 and 2.87 Vs/cm^2 have a continuous mobility distribution. Accordingly $A^+(A^+B^-)_{5bis}$ and $A^+(A^+B^-)_{6bis}$ are absent from the neutralized spray. Although only two doubly charged clusters, $(A^+)_2(A^+B^-)_7$ and $(A^+)_2(A^+B^-)_8$, are easily observed in the non-neutralized spray (Fig. 12, $S = 290$), the existence of many others is probable, since their singly charged daughter products $A^+(A^+B^-)_7$, etc. appear when the spray is neutralized. Fig. 13 is for FOR5 at a smaller liquid flow rate, $Q = 0.109$ nl/s, at which the mean diameter of the drops is of some 36 nm. We shall later argue that the corresponding electric fields on the drop surface are now large enough to suppress most of the Coulomb explosions in the spray. No significant signal of singly charged clusters beyond $A^+(A^+B^-)_8$ is detected in the neutralized spray. No significant signal due to doubly charged clusters is detected either in the original spray (Fig. 13, $S = 290$). This confirms the observations made previously with the TEAOH-THABr solution: doubly charged clusters appear only when the drops undergo Coulomb explosions.

The dependence of clustering on the concentration of THABr is examined in Fig. 14, where another THABr-AcA formamide solution, FOR4, is investigated. While the conductivities of FOR4 and FOR5 are similar, the concentration of THABr is 7 times smaller in FOR4 than in FOR5. For the case of FOR4 and $Q = 0.434$ nl/s, the mean diameter of the original drop is 53 nm. Therefore the evolution of the spray drops will resemble that already described in Fig. 12. However, the spectrum of the neutralized spray detected by the CNC in Fig. 14, $Q = 0.434$ nl/s, is quite different: singly charged clusters beyond $A^+(A^+B^-)_8$ are barely observed. $A^+(A^+B^-)_6$ and $A^+(A^+B^-)_5$ are not detected either, while $A^+(A^+B^-)_{6bis}$ and $A^+(A^+B^-)_{5bis}$ do exist. This means that in the original, non-neutralized aerosol the only singly and doubly charged clusters present are from A^+ up to $A^+(A^+B^-)_4$, and from $(A^+)_2(A^+B^-)_4$ up to $(A^+)_2(A^+B^-)_7$. Such differences between FOR4, $Q = 0.434$ nl/s and FOR5, $Q = 0.284$ nl/s must be due to the different concen-

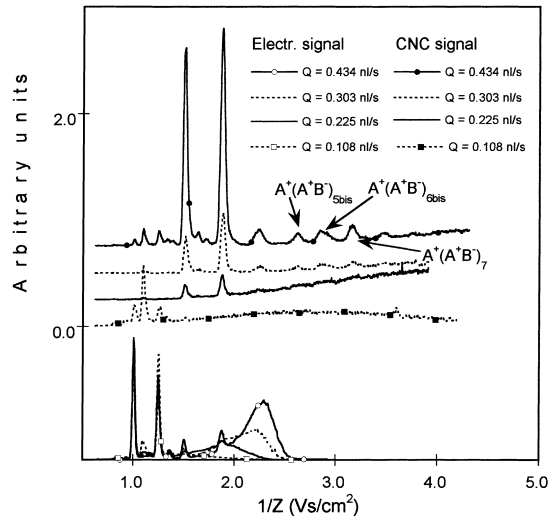

Fig. 14. Illustration of the suppression of Coulomb explosions for solution FOR4 as Q decreases (0.434, 0.303, 0.225 and 0.108 nl/s). The CNC and electrometer lines are for partially discharged and naturally charged sprays, respectively.

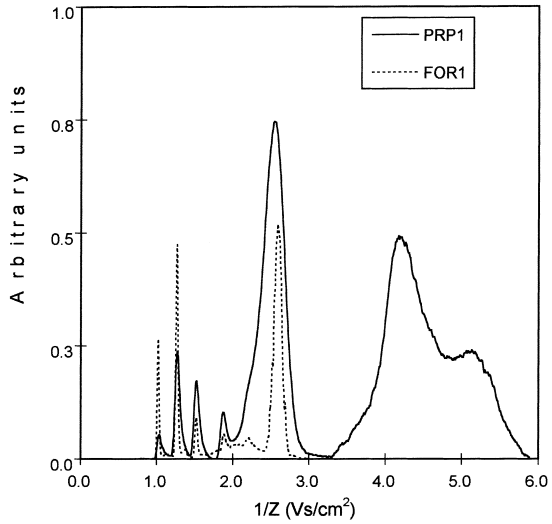

Fig. 15. Electrometer signals vs. inverse mobility for FOR1 and PRP1.

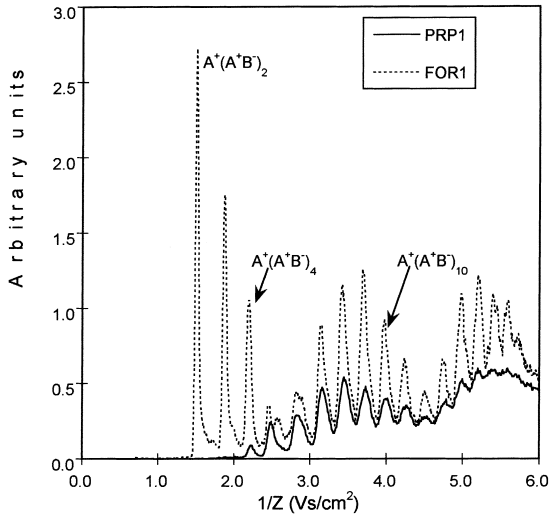

Fig. 16. CNC signals vs. inverse mobility for FOR1 and PRP1 after partial neutralization.

trations of THABr in both solutions. Other three flow rates of solution FOR4, 0.303, 0.225 and 0.108 nl/s, are shown in Fig. 14 as well. The lowest one has an associated mean drop diameter of 33 nm, and the absence of doubly charged clusters is quite clear. Furthermore, as the flow rate is lowered the number of THABr salt molecules available per unit drop charge decreases (see the values of the ratio z/n in Table 2), and the clustering degree should decrease, as observed.

Figs. 15–17 study the dependence of clustering on the nature of the liquid. Fig. 15 shows two curves obtained from the DMA's electrometer for solutions FOR1 and PRP1. Fig. 16 plots the CNC curves after neutralizing the aerosols. Although the residues of both sprays are markedly different, as would be expected from the very different salt concentration and size of the original drops, the same cluster peaks appear in both sprays (note that the smallest clusters are not observed due to the insufficient supersaturation used). Finally, in Fig. 17 different values of S are used to study a non-neutralized spray of PRP1. The phenomenology is quite similar to that described in Figs. 2–4 for solution FOR1, and, in particular, exhibits the same sequence of singly charged clusters.

4. Probing the coulomb explosions via energy analysis

We have made a claim regarding our ability to eliminate Coulomb explosions in drops electrosprayed from sufficiently conducting solutions at small liquid flow rates. This ability is essential to physically suppress Dole's mechanism of ionization, and key aspects of

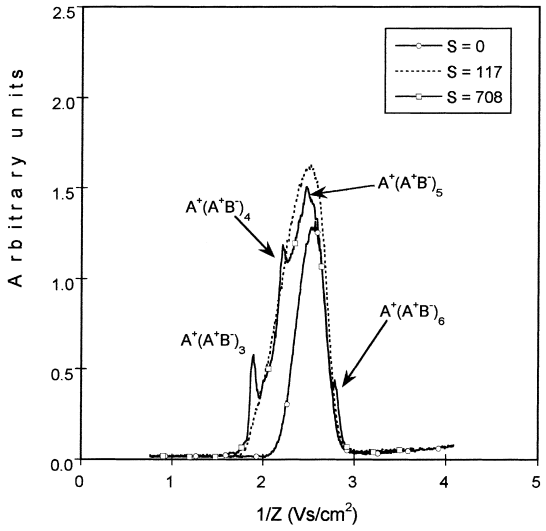

Fig. 17. CNC signal vs. inverse mobility at various PSM supersaturations for a naturally charged PRP1 spray.

our reasoning will depend on its accuracy. The reliability of such a claim must therefore, be firmly established. The radical variation with liquid flow rate Q of the mobility spectra shown in Fig. 9 (solution FOR3) directly demonstrates that a dramatic change of behavior does indeed arise under such conditions. In Section 5 we will argue that these changes in K and Q increase the electric field at the drop surface beyond a critical value at which ion evaporation proceeds fast enough to keep the evaporating drops below the Rayleigh limit. Here we recall the essence of an independent experimental study confirming this point directly [30,32,33].

The occurrence of Coulomb explosions can be monitored via energy analysis of the spray drops in a vacuum. In a nutshell, the drops produced at the tip of the Taylor cone have stopping potentials close to the needle voltage, while the daughter drops produced in flight by their Coulomb fissions are stopped at considerably lower repulsion voltages. Such stopping voltages have been measured with the electrode configuration shown in Fig. 18. The voltage difference required to produce the cone-jet is set between the electrospray needle and an intermediate extractor electrode, and is kept at a constant value at which the cone-jet is stable. The whole spray leaves this inner region through a small orifice drilled on the extractor, and travels toward the collector. The current of charged spray drops reaching the electrometer connected to the collector is measured as a function of the voltage difference between the collector and the needle tip. Fig. 19 includes one series of such stopping potential curves, corresponding to a solution of tributyl phosphate (TBP) with a relatively small con-

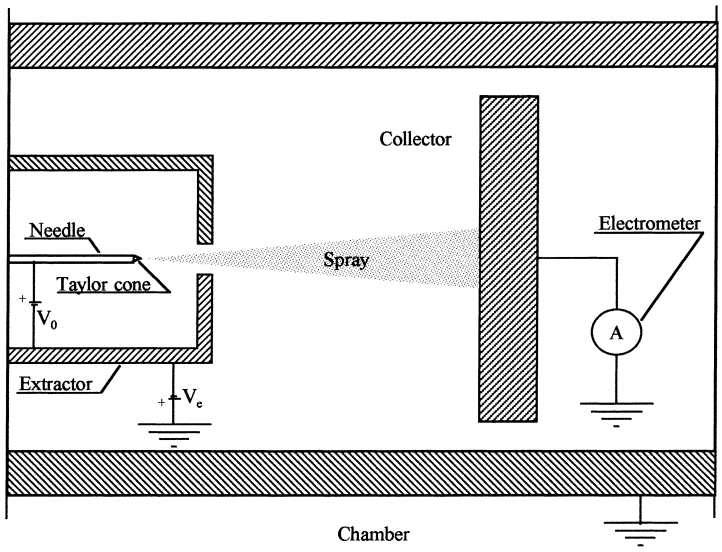

Fig. 18. Electrode geometry used for the stopping potential investigation of electrospray drops.

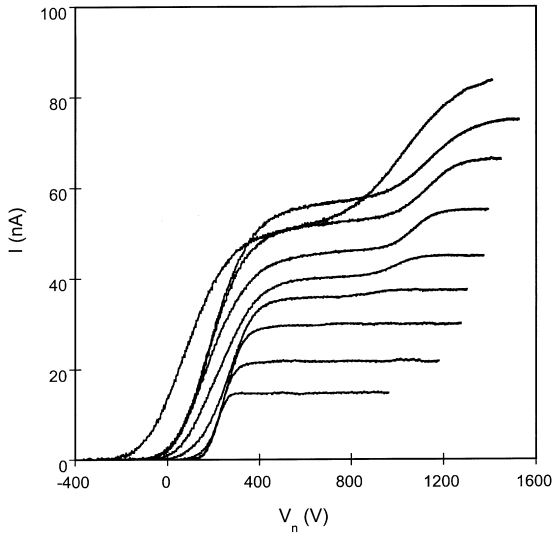

Fig. 19. Stopping potential curves for a solution of tributyl phosphate, at different liquid flow rates. Electrical conductivity $K = 4.40 \times 10^{-4}$ S/m. V_n is the potential difference between the electrospray needle and the collector electrode. Notice the second step arising when $I > 30$ nA, due to in-flight Coulomb explosions.

ductivity of 4.40×10^{-4} S/m, at nine different values of the liquid flow rate. The curves have a single step at the lowest flow rates, implying that the spray is formed by drops of only one type, all released at the jet break-up. For sufficiently larger flow rates, a new step appears at larger voltages, while the left tails of the curves broaden and shift to lower voltages. The high voltage step to the right is associated to the small daughter drops produced in Coulomb explosions. The broader peak at the left is a superposition of the steps associated to drops which have not exploded and to mother drops from the explosions (the top curve has a more complex structure due to instabilities arising in the cone-jet at the largest flow rate, which are irrelevant to the present discussion). Note that the drops explode because they are produced initially with a net charge larger than Rayleigh's; not due to solvent evaporation, which is unimportant due to the short flight times. However, if the drops had an alternative mechanism to shed excess charge, they would no longer explode, and this could be immediately observed through the disappearance of the second step.

The electrical conductivity of the solution of TBP just discussed is too small for ion evaporation to play any role. But we have used a modified version of this set-up intended to measure directly ion field evaporation rates from highly conducting cone-jets of formamide. Depending on the electrical conductivity of the solution and its flow rate, ions could evaporate from the meniscus surface, as well as from the spray drops. By isolating the current of ions produced at the meniscus, we have determined ionization rates which do support quantitatively the notion that these ions are field-evaporated a la Iribarne and Thomson [33,30]. Simultaneously, one sees the disappearance of the second step in Fig. 19.

Fig. 20 shows stopping potential curves for a NaI–formamide solution with $K = 0.207$ S/m. The second steps associated to daughter drops from Coulomb fissions are present at all flow rates, even the smallest one. Fig. 21 is for a solution with $K = 1.42$ S/m, and shows the conspicuous absence of the second step at all flow rates. Two features worthy of note new are that: (a) the current measured at the collector is negative at low voltages. (b) the current detected above 800 V keeps growing slightly. These two characteristics are actually due to secondary ionization prompted by surface collisions of the ions evaporated from the meniscus and the spray drops [33,30]. Fig. 22 shows stopping potential curves for an intermediate conductivity, $K = 0.715$ S/m. Although Coulomb explosions are detected above $I = 130$ nA, they disappear at the

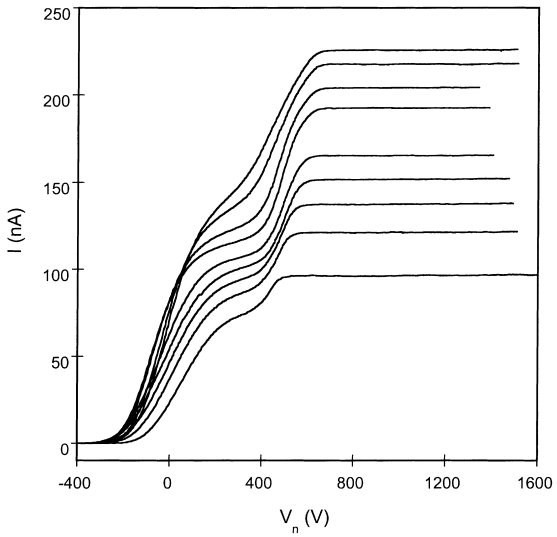

Fig. 20. Stopping potential curve for a NaI–formamide solution at $K = 0.207$ S/m showing explosions at all flow rates.

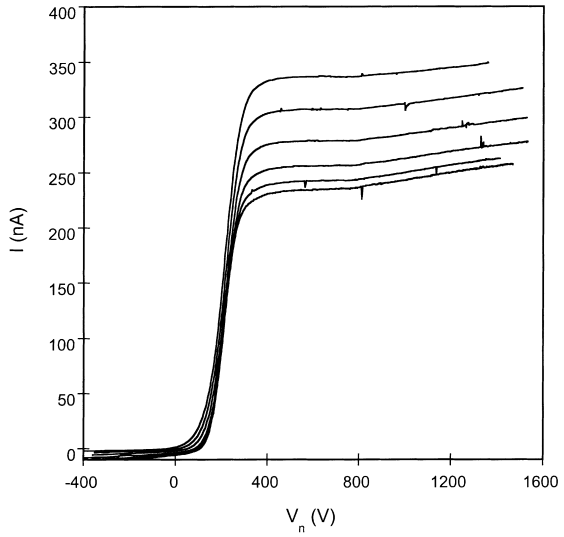

Fig. 21. Stopping potential curve for a NaI–formamide solution at $K = 1.42$ S/m showing no explosions at all.

lowest flow rate. This behavior is to be expected qualitatively from the IEM, since higher K and smaller Q values lead to the production of smaller drops sustaining higher fields on their surface. If there is a certain critical E^* at which ions begin to evaporate, then there is a certain drop diameter at which E^* is reached at

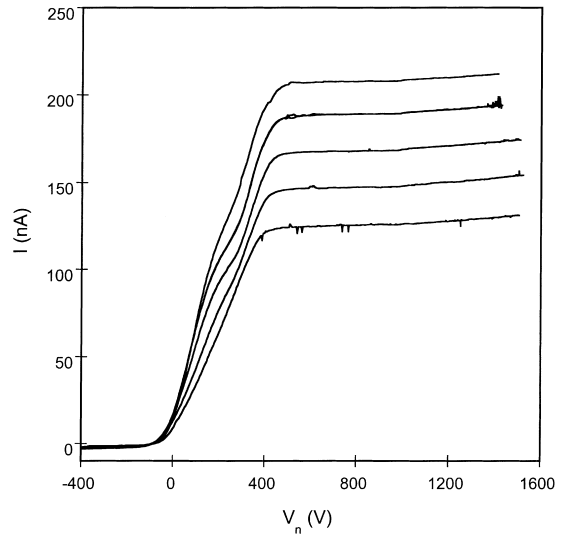

Fig. 22. Stopping potential curve for a NaI–formamide solution at $K = 0.715$ S/m showing exhibits a transition between these two behaviours as the flow rate decreases.

birth, and there must be a critical K, Q pair able to create such small drops. Therefore, drops produced at K and Q below this critical value, although born with a net charge above their Rayleigh limit, will avoid the Coulomb explosion by the simple procedure of evaporating their charge.

5. Discussion

5.1. The nature of the clusters

We have made no mass spectrometric study of these clusters. However, as reasoned below, there is little ambiguity about the assignment made in Table 3 of a charge state z and aggregation level n to each of the discrete peaks of singly and doubly charged clusters observed in the mobility distributions.

The largest singly charged cluster present in the non-neutralized spray ($Z^{-1} = 2.83$ VS/cm^2) is activated in the PSM at $S = 290$, while a doubly charged ion with a similar mobility is activated at $S = 100$. This large difference in critical supersaturation therefore, fixes z unambiguously [28]. Less evident but also unambiguous is the assignment of n. A number of authors have studied previously electrosprays of tetraalkyl ammonium salts by mass spectrometry. The dominant peak is the bare A^+, with the dimer $A^+(A^+B^-)$ and in some cases also the trimer $A^+(A^+B^-)_2$ being also relatively prominent. Siu and colleagues [34] have measured ion mass and mobility in series for several such salts (5 mM in 50–50 water–methanol). For tetraoctyl ammonium bromide they confirm that these three clusters appear dominantly in both the mobility and the mass spectra. Our whole $z = 1$ series can then be constructed by just counting from the most prominent and mobile ion, labeled $n = 0$.

The situation is slightly more complicated for the doubly charged series. Its first member is already in a relatively high state of aggregation, and we are not aware of its prior mass spectrometric observation, even though its m/z falls surely within the range of many mass spectrometers. However, once one doubly charged ion peak is assigned to an n value, the remaining ones follow also just by counting.

Fig. 23 shows the inverse mobility of singly charged ions and twice that of doubly charged ions as a func-

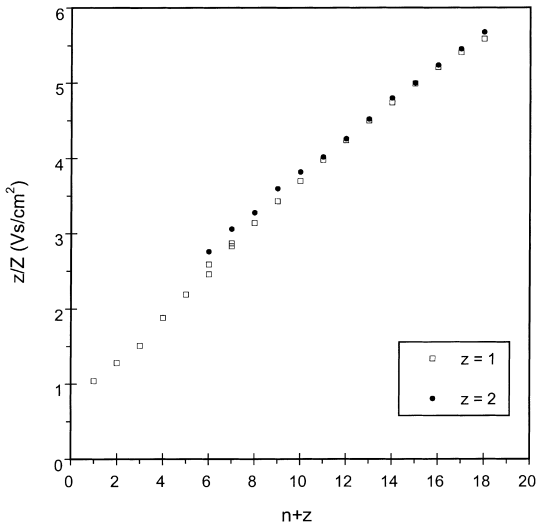

Fig. 23. Inverse mobilities for singly and doubly charged clusters $(A^+)_z(A^+B^-)_n$ of tetraheptyl ammonium bromide (A^+B^-) in air.

tion of their number of tetraheptyl ammonium groups (n+z). For the singly charged series we represent the non-neutralized ion mobilities for $n+z \leq 7$, and the neutralized ion mobilities for $n+z=6$. Both types of data are available only for $n+z=6$ and 7 only. One can see a small discontinuity between the neutralized and non-neutralized series, corresponding probably to the fact that the neutralizing anion N^- attaching to the cluster has a volume larger than that of the Br^- it displaces. The choice of $(n+z)$ over n follows from the fact that the volume of the cation is much larger than that of Br^-, so that the volume of the molecule is approximately proportional to $(n+z)$. The most mobile doubly charged ion is $(A^+)_2(A^+B^-)_4$ with very high probability. With this choice, the match between the two curves beyond $(n+z)=11$ is as good as can be expected from the accuracy of this measurement technique. Below $n=11$, the drag z/Z of the doubly charged series exceeds increasingly that for $z=1$, even though these ions are smaller than the singly charged ones (they have one less Br^- atom than the non-neutralized singly charged clusters and one less neutralizing anion N^- than the neutralized series). The higher drag of the smaller doubly charged clusters must hence follow from the increased cross-section due to ion-neutral polarization interaction associated to the higher charge. Since the doubly charged ions are smaller than singly charged ions with the same $n+z$, the increase in drag due to polarization is actually larger than the vertical shift seen between the +and ++series of Fig. 23. As expected, the polarization contribution to the drag decreases (at constant charge z) with increasing ion diameter. We are not aware of any prior measurement of this effect for two such small and nearly identical clusters at two different z values.

The possibility exists that a peak from an impurity might have sneaked into the series, thereby displacing all the larger ions. Such an effect can be readily spotted by a discontinuity in the otherwise smooth $Z(n)$ curve, as well as by a mismatch between the curves for $z=1$ and $z=2$. For instance, of the two close doubly charged peaks arising at $1/Z=1.87$ and 1.91 (Fig. 2), only the second is included in Fig. 23. The two correspond most likely to a pair of different conformations of $(A^+)_2(A^+B^-)_8$. This is the only case of doubly charged ions found where two similarly abundant conformers were observed. An anomalous singly charged peak appears at 1.39 Vs/cm^2 Fig. 4), probably due to an impurity in the sample.

Other series of clusters with three, four ... charges are present in the original spray (see, for instance, Fig. 2, $S=68$). Unfortunately, as the charge state increases, they tend to concentrate into a relatively narrow range of mobilities. Consequently, the present experimental technique has a high risk of missing some peaks from each z-series, and may lead to unreliable results. The clusters holding more than two charges can be unraveled by use of two DMAs in series with a neutralizer placed in between. We have used this technique to confirm the existence of clusters with all charge states from one to nine in the mobility range $1.40\ Vs/cm^2 < Z^{-1} < 2.90\ Vs/cm^2$ [30]. This method also proves that the clusters identified here as $(A^+)_2(A^+B^-)_4$ to $(A^+)_2(A^+B^-)_{17}$, are indeed doubly charged.

5.2. The pure charged residue mechanism (CRM)

Let us define here the ‘pure Dole ionization mechanism’ [35], or ‘pure CRM’, as one in which the only means by which an evaporating drop of diameter D may loose charge is via Coulomb explosions arising when its charge q approaches the Rayleigh limit q_R [36–38]:

$$q_R = \pi(8\gamma\varepsilon_0 D^3)^{1/2} \quad (3)$$

where γ and ε_0 are the surface tension of the liquid and the vacuum permittivity, respectively.

Fenn et al. [39] have argued in considerable detail why this pure mechanism raises too many paradoxes to be credible, at least in the case of relatively small ions. Their cogent rejection of this 'pure' mechanism is strongly and quite directly confirmed in Fig. 9, which shows that ions are created even when there are no Coulomb explosions. These drops must therefore, have a means other than Coulomb explosions to shed charge, and they clearly do so by ejecting bare solution ions (perhaps solvated) and relatively small singly charged clusters with n £ 6. We will follow Iribarne and Thomson in referring to this alternative ionization mechanism as the ion evaporation mechanism (IEM). Its existence is strongly and independently confirmed by the fact that Coulomb explosions may be suppressed in the case of sufficiently small initial drops. This plainly means that, as the solvent evaporates, the drops can rid themselves of charge at a rate large enough to remain below the Rayleigh limit. A clear distinction must be made here between ion evaporation, Coulomb explosions and the hypothetical microexplosion of Rollgen and others. Two radical differences between Coulomb explosions and ion evaporation are that the first mechanism occurs only at the Rayleigh limit and never below, and is an exothermic process. Ion evaporation is an activated process with a large activation energy (∼2 eV) and may occur below the Rayleigh limit. In addition, Coulomb explosions produce drops of macroscopic size [40–43]. The notion that Coulomb explosions could as easily eject drops 1–2 nm in diameter is unfounded and must be discarded. Such a nano-emission would be an activated process governed by Iribarne–Thomson kinetics, and distinguishable from ion evaporation only in that the activation energy would be considerably larger than 2 eV (as easily seen via the Born model).

Before moving on to the IEM, we should note that the 'pure Dole' mechanism just rejected is a radicalization of what Dole and his colleagues proposed. The notion that evaporation accompanied by a sequence of Coulomb explosions leads to smaller and smaller drops is undeniable. In fact, Nohmi and Fenn [44] have argued that Dole's mechanism is responsible for the formation of multiply charged polyethylene glycol ions with molecular weights in the range of 1 million. Other instances where either highly charged colloidal nanoparticles [45] or singly charged macromolecules [46–48] were also undoubtedly produced via CRM have been discussed in the literature. In a companion paper we analyze the importance of Dole's mechanism in the formation of ions of globular proteins [49]. But there is more. Fig. 11 shows that neither doubly charged cluster ions of any size, nor singly charged ions with $n = 7,8,9,...$ are produced when Coulomb explosions are suppressed. Yet, many of these clusters are abundantly formed in the presence of Coulomb explosions. It is therefore, clear that some form of 'impure' Dole mechanism must play a leading role also in the formation of clusters with diameters as small as 2 nm, and perhaps smaller. The various pieces of evidence brought so far by other researchers to defend the role of either the IEM [39] or variants of the charged residue mechanism [12–20] in the formation of cluster ions from electrosprays are therefore, not mutually exclusive. What we see here cannot be fully explained by either pure IEM or pure CRM, but becomes easily understood as a result of both mechanisms acting in concert.

A final point worth stressing is that the pure Dole mechanism tends to form residues charged typically between 70% and 100% of the Rayleigh limit (based on the surface tension of the solvent–solute system). Indeed, it is generally thought that a drop undergoing one such fission ejects a relatively large number of smaller drops carrying collectively some 15% of the initial charge and only some 3% of its initial mass (for recent reviews on the related literature, see [40,41]). This would leave the initial drop charged at around 89% of q_R. The most extreme situation one may conceive is one in which a Rayleigh fission divides a drop into just two fragments, each carrying half of the initial charge and volume, and being hence left at 70.7% ($2^{-1/2}$) of q_R. In either case, the main products of a succession of Rayleigh fissions would always be charged between 70.7% and 100% of q_R. No measurements are available on the number of daughter drops produced in Coulomb explosions, nor on their charge. However, when many daughters are formed per fission, this involves almost surely the formation of a cone-jet and its break-up into drops [40,50]. The charge on these drops must therefore, be that of drops formed in Taylor cone-jets, whose mean charge is known to be typically $0.7q_R$ [42,43]. Alternatively, if only two or a few daughter drops were formed, we would approach

the situation already discussed when they would hold at formation 70.7% of q_R. In conclusion, most of the drops produced in the pure Dole mechanism hold at all times charges comparable to q_R. This applies also to the residues left after their final evaporation, implying that clusters charged well below the Rayleigh limit (of a solvent drop of the same diameter) cannot originate via the pure CRM.

Another important role of the repeated Coulomb subdivision of charged drops is to increase the z/n ratio in the daughter drops and decrease it in the parent. This mechanism has been analyzed in detail in earlier work from the groups of Kebarle and Cole, and, when present, is clearly able to produce charged drops with z/n ratios close to unity. This charge-enrichment process is most effective for surface active ions, but it operates quite generally as a result of the fact that q/m is considerably higher in the daughters than in the mothers of a Coulomb explosion.

5.3. The ion evaporation model (IEM)

A variety of ionization mechanisms could conceivably be put forward to explain our observation that drops shed charge by means other than by Coulomb explosions [51–53,54,20]. However, the only model where the process has been described in sufficient detail to allow predictions of the ionization rate is that of Iribarne and Thomson. They treated the desorption of ions from liquid surfaces as a kinetic process where the escaping ion has to overcome a potential barrier, Δ, located at a given distance, y^*, above the liquid surface. The flux of evaporated ion charge, j'', can be written as

$$j'' = \frac{kT}{h}\sigma \exp\left[-\frac{\Delta}{kT}\right] \tag{4}$$

where σ stands for the surface charge density (C/m^2). When the radius of curvature of the surface, R, is very large and there is no electric field, Δ coincides with, ΔG_S^0, the solvation free energy of the ion in whatever state of solvation it happens to be evaporated. In general, however, Δ is known to be reduced by the presence of an electric field E on the drop surface. We argue in the Appendix A that Δ is also significantly affected by the finite curvature of the drop. The IEM hence remains incomplete until Δ is specified as a function of E and R (perhaps also other variables defining the ion and its interaction with the solvent):

$$\Delta = \Delta(R, E) \tag{5}$$

Iribarne and Thomson determined the far field of the ion–liquid attractive interaction by reducing it to the polarization potential between a point charge and a dielectric sphere. They accounted for the effect of curvature in the repulsive Coulombic field from the charged drop, but not in the attractive polarization potential. They further had to use an origin for the potential energy, which they took to vanish one ionic radius within the liquid bulk. However, the corresponding energy shift was too large because they took the electric field E_i inside the dielectric as equal to its value E in the gas side. In spite of these shortcomings, they obtained an expression for Δ as a function of z, R and the dielectric constant ε of the liquid. By comparing the characteristic time for ionization to that for solvent evaporation they found reasonable values for the electric fields and drop diameters required for evaporating small ions and their model has been widely (though not universally) accepted by subsequent authors.

Loscertales and Fernández de la Mora [31] first noticed the curvature and the energy origin deficiencies in the original Iribarne-Thomson model for Δ. In order to sidestep these problems they chose to ignore altogether the effect of curvature under the assumption that it would be small for their drops, having diameters typically larger than 20 nm. They also restricted their study to liquids with high dielectric constants, $\varepsilon \gg 1$, for which the Iribarne–Thomsom energy shift inside the drop is essentially negligible because the electric field is ε times smaller inside than outside the liquid, $E_i = E/\epsilon$. The resulting polarization potential then degenerates numerically into the image potential with net external field E (yet is physically quite different from the image potential; [31]):

$$W(y) = C - \frac{e^2}{16\pi\varepsilon_o y} - Ey; \quad y \gg 1\,\text{Å} \tag{6a}$$

where e is the unit charge, y the distance from the wall, E the electric field at the gas side of the interface, and the constant C is chosen such that the origin of energies is on the liquid surface. Evidently Eq. (6a) is only a far-field approximation to the real potential energy, valid for values of y larger than the ion diameter and the range of interatomic forces. For values of

y of the order of atomic dimensions Eq. (6a) must be substituted by

$$W(y) = \phi(y) - Ey \tag{6b}$$

where the interaction energy $\phi(y)$ vanishes (by choice of the origin) at the interface $y = 0$, and asymptotes into the image energy when y is larger than the ion radius:

$$\phi(y) \to C - \frac{e^2}{16\pi\varepsilon_0 y}; \quad y \gg 1\,\text{Å} \tag{6c}$$

At the maximum of (6a) one finds for Δ and y^*:

$$\Delta = C - \left(\frac{e^3 E}{4\pi\varepsilon_0}\right)^{1/2}; \quad y^* = \left(\frac{e}{16\pi\varepsilon_0 E}\right)^{1/2} \tag{7,8}$$

The meaning of the constant C is readily grasped because, in the absence of electric field E, Δ is just the solvation energy ΔG_S^0 of the ion. But Δ is also equal to C according to (7), so that

$$C = \Delta G_S^0 \tag{9}$$

Eq. (7) implies that the electric field reduces the activation energy through the so-called Schottky hump $(e^3E/4\pi\varepsilon_0)^{1/2}$. Notice for reference that, when $E = 1\,\text{V/nm}$, y^* takes a value of 0.44 nm, a distance from the interface sufficient for the use of the asymptote (6c) to be reasonable in the case of small ions.

Using the fact that the ion evaporation rate depends exponentially fast on E while the rate of solvent evaporation is approximately constant, it was argued in [31] that the electric field on the liquid surface would be approximately constant, its value being inferred from the charge and diameter of the solid residues, measured with a DMA and an inertial impactor. They also inferred the ion evaporation rate from the calculated rate of solvent evaporation and the approximate condition that E is constant, from which they determined Δ in (4). They could then compare this value with that predicted in (7), and did find an excellent agreement for several small inorganic ions in aqueous solution.

The maximum residue mobility observed in the electrosprays of [31] was found to be independent of the liquid flow rate and the electrical conductivity of the solutions. This was explained as resulting from the expected constancy of the surface electric field, since $E \sim z/D^2$, which they thought was proportional to the mobility Z. However, more recent work has led to the realization that the shift of d_0 arising in Eq. (1) is by no means negligible and destroys the strict proportionality between Z and E. Furthermore, in a subsequent unpublished study, Loscertales (1996) noticed a systematic increase in the mobility of these residues as their diameter decreased, whereby the corresponding surface field also increased. In other words, the independence observed earlier between $Z_{\max}$ and liquid conductivity or flow rate was an artifact of the fact that Z was always measured at the tail of the distribution, and this extreme mobility was indeed invariant. But less mobile particles produced in the same spray seemed to have a smaller associated value of E.

These paradoxical results were confirmed in a considerably more detailed and precise study by de Juan [55]. He selected particle residues of given mobility and determined their mass by means of a focusing impactor. For aqueous solutions of tetrabutyl ammonium bromide, he found the following striking results: independently of liquid conductivity and flow rate the residues of the electrosprayed drops were such that at a given diameter they always carried nearly the same charge, $D = D(z)$. Furthermore, residues with diameters larger than 32 nm were at a constant fraction of q_R (~64% in all cases based on the surface tension of pure water). Below 32 nm there was a break in his $D(z)$ curve which could be interpreted as due to the onset of ion evaporation. This happened at a field of $E = 1\,\text{V/nm}$, comparable to values inferred by others [8–11,31,56,57]. However, following this discontinuity in the slope, E continued increasing at decreasing diameters, reaching a value of some 1.2 V/nm at $D = 8$ nm. The change between 1 and 1.2 V/nm may not appear as sufficient grounds to worry. But the reproducibility and accuracy of the results was more than enough to make such differences highly significant. Although the data interpretation was also based on the inaccurate assumption that $d_0 = 0$ in (1), we find that these conclusions are qualitatively unchanged after introducing this correction.

In conclusion, the remarkable fact that there is a strict $q(D)$ relation different from $q_R(D)$ shows that there is a new mechanism for charge loss which differs below 32 nm from the Rayleigh fission process. However, the $q(D)$ relation found is not that $E =$ constant, as expected from the work of Loscertales and Fernández de la Mora. Something is therefore, missing from their model.

Table 4
Field ionization function $F(z)$ defined in equations (A5), (A8)[a]

z	1	2	3	4	5	6	7	8	9	10
$x^*(z)$	1.6180	1.4276	1.3434	1.2936	1.2600	1.2354	1.2164	1.2012	1.1888	1.1783
$F(z)$	0.5000	0.8354	1.1111	1.3515	1.5677	1.7658	1.9498	2.1224	2.2855	2.4404

[a] x^*/R is the dimensionless distance to the center of the sphere where the top of the potential barrier is located.

This paradoxical situation has perplexed us until the recent realization by Gamero–Castaño [30] that the effects of curvature on Δ are of a magnitude sufficient to explain the observed dependence of the electric field on the radius of the evaporating drop. This point may be readily demonstrated by means of models that account for the curvature, as shown in the Appendix A. The result can be cast into the form

$$\Delta = \Delta G_S^0 - \frac{e^2}{4\pi\varepsilon_0 R}[F(z) + \alpha] \tag{10}$$

where the function $F(z)$ is determined from (A5) and (A8), with numerical values shown in Table 4 for integer values of z from 1 to 10. Its asymptotic value for large z is given in the Appendix A, Eq. (A9). α is a dimensionless ion solvation energy shift constant which approaches the value 5/8 for very small ions, and is zero if one takes the energy of solvation of the ion to be independent of drop curvature.

On their way to show that E is approximately constant during the ion evaporation process, what Loscertales and Fernández de la Mora really showed is that the exponent Δ/kT must take a certain critical value. In its simplest rendition, the argument goes as follows: The ionization rate varies as $\exp[-\Delta/kT]$. Since $\Delta G_S^0/kT$ is a large quantity typically of the order of 100, this exponential factor is astronomically small, and no significant ionization will exist unless Δ decreases by an amount comparable to itself. Ignoring curvature and using (7), this simply means that the group $\beta = (e^3E)^{1/2}/[kT(4\pi\varepsilon_0)^{1/2}]$ must itself be large. Now, if E increases by a relatively small amount dE (d$E/E \ll 1$), the exponent β increases by the amount $\beta(\mathrm{d}\ln\beta/\mathrm{d}\ln E)(\mathrm{d}E/E)$. But the logarithmic derivative $(\mathrm{d}\ln\beta/\mathrm{d}\ln E)$ is of order one (1/2 in this case), so that the variation in the exponent is of the order of β times larger than the relative variation in the field. Since β is large, this means that very small relative changes in the field lead to large changes in the exponent and thus exponentially large (hence astronomical) changes in the rate. But if the ionization rate grows astronomically the drop charge will decrease drastically and the rate will become negligible again. The only way in which the process may be settled is by keeping the exponent very close to a certain critical value Δ^* at which the evaporation of ions proceeds at just the rate required to keep the exponent constant as the solvent evaporates. Obviously, the argument can be carried over to the case when the exponent depends both on E and R. The reason is that the exponent remains a large quantity, and its logarithmic derivative with respect to both R and E will remain of order one.

In conclusion, in the model (7), which ignores curvature, Δ depends only on E, and the criterion that Δ reaches the critical value Δ^* implies a constant field $E = E^*$. But once Δ depends both on E and R, the critical condition that $\Delta = \Delta^*$ implies that E and R (or z and R) must be in a certain relation,

$$z = z(R) \quad \text{during ion evaporation} \tag{11}$$

which may differ from the fixed field condition $z/R^2 = \text{Constant}$. This is exactly what was observed experimentally in [55]. The model results (10) provide a concrete form for this relation

$$\frac{4\pi\varepsilon_0 R(\Delta G_S^0 - \Delta^*)}{e^2} = [F(z) + \alpha] \tag{12}$$

5.4. Ion evaporation and the minimum and maximum z of a charged residue

The process of ion evaporation rules directly the types of ions that may be ejected from the drops. In addition, it may also reduce well below the Rayleigh limit the charge level remaining on the residues, thereby fixing the maximum and minimum charge that can be carried by clusters produced by Dole's mechanism. Whatever the actual form of the $z = z(R)$ curve is for drops in the ion evaporation regime, certain consequences follow from the mere fact that

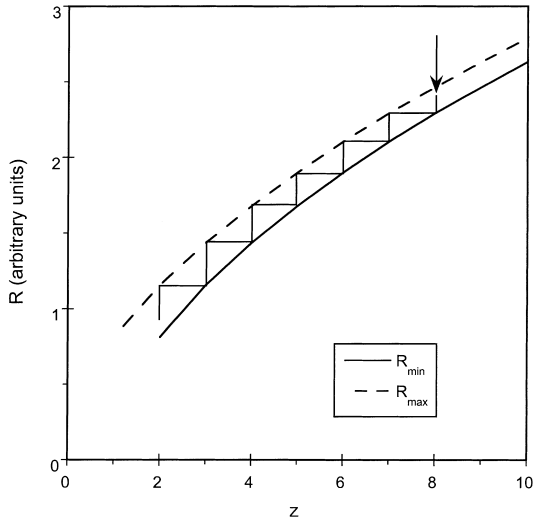

Fig. 24. Maximum and minimum radii that a charged residue carrying z charges may have in the ion evaporation regime. The two curves are shifted horizontally from each other by a unit charge.

such a relation exists. Let us assume that a drop carrying z elementary charges and having a certain radius R evaporates its liquid phase without charge emission provided that the exponent $\Delta(z, R)$ is above a certain critical value Δ^*. Since Δ decreases with increasing charge and decreasing radius, this means that z remains constant while R decreases by solvent evaporation, provided that R is above a certain critical curve $R = R^*(z-1)$.[1] This is shown in Fig. 24 in the vertical line above the line labeled $R_{\min}$:

$$R_{\min}(z) = R^*(z-1) \tag{13a}$$

At the point of intersection of these lines, the drop ejects one charge with very little mass loss, effectively moving horizontally to the left into the point labeled $R_{\max}$ in Fig. 24:

$$R_{\max}(z-1) = R^*(z-1) \tag{13b}$$

There it will continue evaporating at constant z, until reaching again the critical curve, loose one charge, and so forth. Except for the initial long vertical descent in the graph, it is clear that $R(z)$ is always bound between the two curves $R_{\min}(z)$ and $R_{\max}(z)$. Therefore, when the evaporation process is terminated by exhaustion of the liquid, the final residue formed will also lie within these very bounds.

A verifiable predictions of this ion-evaporation-controlled charged-residue mechanism is that the maximum radius of a cluster holding z charges should be close (± 1 salt molecule) to the minimum radius of a cluster holding $z+1$ charges:

$$R_{\max}(z-1) \sim R_{\min}(z) \tag{14}$$

In other words, the respective ranges of radii of clusters having charges z and $z+1$ are contiguous to each other, without either overlapping or leaving empty spaces in between. Since mobility and radius are closely related quantities for particles holding the same charge, once the cluster charge has been reduced to $z=1$ via neutralization, what has just been said about their radii holds equally for their mobilities. Consequently, the mobility spectra of such neutralized clusters should exhibit a modulated sequence of peaks, each initial charge state being perfectly separated in mobility from the two neighboring initial charge states. This is in fact observed in all the figures where a sufficient level of neutralization was reached, particularly in Figs. 6, 7, 11, 12 and 16. For instance, Fig. 6 shows on the left a group of peaks with a maximum at $n=2$ and a minimum at $n=5$ or 6. There is then a second group starting immediately to the right of the previous group, peaking at $n=9$ and ending at a minimum at $n=12$. This is followed immediately by a third group peaking at about $n=15$ or 16, and extending slightly beyond the range of the measurement, up to about 6 Vs/cm^2 ($n \sim 19$). The same effect is seen in the less crowded spectra of Fig. 12 ($S=480$) and Fig. 16. Direct observation of the charge states (Fig. 2) shows that the first two modulated waves correspond to $z=1$ and $z=2$, and it is natural to assume that the third group originates in triply charged particles. The remarkable experimental observation that these various groups of peaks are so neatly juxtaposed provides a rather strong confirmation of (14). Such a regular pattern would be unthinkable if these clusters originated from the highly random dynamics of Coulomb explosions envisioned by Dole.

[1] Notice that the critical condition (12) is based on the number of charges $(z-1)$ after the drop emits one ion.

5.5. Suppression of Coulomb explosions

Coulomb explosions have been seen to be suppressed in a variety of circumstances and by a diversity of methods. We have argued qualitatively that this happens when the field on the drop surface is large enough. Let us now do so more quantitatively. Whenever a drop reaches the ion evaporation regime it ceases to undergo Coulomb fissions. This was seen by de Juan [55] to happen for water-tetrabutyl ammonium at a diameter of 32 nm and an electric field of 1 V/nm. His drops were originally larger than this critical diameter and hence did initially undergo a certain number of such fissions. However, if one manages to produce drops with initial diameters that put them in the ion evaporation regime before their first fission, then they will never explode. The conditions for this to happen can be calculated from available scaling laws on the mean diameter and charge of the drops initially produced by a Taylor cone-jet. These laws were initially proposed by our group [58,59], but have been since confirmed by experiments in two other laboratories [60–62]. The spray current I and mean drop diameter $\langle D\rangle$ obey:

$$I = f(\varepsilon)\left(\frac{\gamma Q K}{\varepsilon}\right)^{1/2}; \quad \langle D\rangle = g(\varepsilon)\left(\frac{Q\varepsilon\varepsilon_0}{K}\right)^{1/3} \tag{15,16}$$

where the most up-to-date experimental values of the functions $f(\epsilon)$ and $g(\epsilon)$ are 24.7 and 0.80, respectively, for the case of formamide ($\varepsilon = 110$) [61]. The electric field on the drop surface based on their mean diameter and charge can then be written:

$$E \sim \frac{I D}{6\varepsilon_0 Q} = \frac{f(\varepsilon)g(\varepsilon)}{6}\left(\frac{\gamma^3 K}{\varepsilon\varepsilon_0^4 Q}\right)^{1/6} \tag{17}$$

Hence, E can be raised by increasing the conductivity K of the solution, as well as by decreasing Q, though there is a minimum flow rate, $Q_{\min} \sim 1/K$, below which a cone-jet cannot be stabilized. Therefore, by designing a solution with an electrical conductivity such that Coulomb explosions are suppressed at flow rates somewhat larger than the minimum, one should be able to observe the transition between both regimes by just varying Q. This is actually what is found by stopping potentials in Fig. 22. For the lowest curve, where Coulomb explosions are eliminated, the critical flow rate, measured current, estimated mean drop diameter and its associated electric field are 0.0634 nl/s, 124 nA, 36 nm and 1.27 V/nm, respectively. $\langle D\rangle$ and E are quite comparable with the values mentioned earlier from [55] ($\langle D\rangle = 32$ nm; $E = 1$ V/nm). They are also close to those at which the mobility spectra of FOR3 undergo the radical transformation shown in Figs. 9–12 ($Q = 0.0958$ nl/s: $I = 188$ nA, $\langle D\rangle = 34$ nm and $E = 1.28$ V/nm). We are here dealing with three rather different experimental situations and measurement methods in which a drastic change of behavior is seen in either a $q(D)$ curve, a stopping potential curve or a mobility distribution. They all happen under conditions at which one would expect the onset of ion evaporation if the IEM were to apply.

5.6. The ionization mechanism for the various clusters

We have shown that the doubly charged clusters appear only when the spray drops undergo Coulomb explosions. When such fissions are greatly reduced (Fig. 13) or completely suppressed (Fig. 14 and bottom line of Fig. 11), the peaks of doubly charged ions become barely distinguishable, or disappear entirely. These clusters are therefore, not field evaporated from the liquid drop. Instead, they are produced by a combination of CRM and IEM, in the sense that the clusters are the final stage of evaporating liquid droplets which have lost most of their net charge by ion field desorption. Their final charge is therefore, fixed by the IEM.

On the other hand, singly charged clusters can in principle be produced by both mechanisms. They clearly can be field evaporated, since they appear in sprays where Coulomb explosions are absent. Under these conditions we have experimentally detected (Fig. 11) all the ions in the series $A^+(A^+B^-)_n$ from $n = 0$ to $n = 5$. The cluster $A^+(A^+B^-)_6$ absent from the figure is formed abundantly in electrosprays of solutions containing higher concentrations of tetraheptyl ammonium bromide Figs. 3 and 4). One can in fact argue that this cluster is also formed exclusively by field evaporation. For if it were produced as a charged residue, it would have to come from a drop containing the substance necessary to create the cluster $(A^+)_2(A^+B^-)_6$ and having subsequently evaporated

one charge. The existence of such drops in the spray of Fig. 14, $Q = 0.434$ nl/s, follows from the presence of $(A+)_2(A^+B^-)_6$, inferred from the peak of its partially neutralized daughter product $A^+(A^+B^-)_7$. But if $A^+(A^+B^-)_6$ itself does not form even when its precursor $(A+)_2(A^+B^-)_6$ is clearly present, it is evident that a drop containing two A^+ ions and six molecules of tetraheptyl ammonium bromide is stable and will not lose one charge. $A^+(A^+B^-)_6$ cannot be, therefore, created as a charged residue, and its presence in some of the sprays shows that it is field evaporated. The reasons why this cluster does not form (field evaporate) from solution FOR4 is probably that it does not pre-exist in this relatively dilute solution.

It would be interesting to determine how small is the smallest singly charged residue that can be formed via Dole's mechanism. This would illustrate further the tremendous power of drop subdivision inherent to a cascade of Coulomb fissions, which we already know can form clusters at least as small as $(A^+)_2(A^+B^-)_4$, with a mobility diameter smaller than 1.9 nm. Unfortunately, since all the singly charged ions with diameters smaller than $(A+)_2(A^+B^-)_4$ are produced by field evaporation, it is not possible under our working conditions to determine whether or not they are also created by the CRM.

5.7. Structure of the mobility distributions

We are now in a position to unravel the triple structure observed in the mobility distributions. For the relatively large particles activated at $S = 0$, one sees two peaks in Fig. 2: one above 2.4 Vs/cm^2 (mode I) and another from Z^{-1} from 2 to 2.4 Vs/cm^2 (mode II). The third mode detected at larger saturations below 2 Vs/cm^2 is clearly due to very small particles and clusters (mode III). There are in addition the sharp peaks associated to singly charged ions formed directly by field ionization.

The low mobility mode *I* extends in some cases to fairly large Z^{-1} (Fig. 8), and is sometimes narrow (Fig. 2), but is lost entirely in the absence of Coulomb explosions. Although the residues from this mode have not been investigated directly here, they seem to proceed from drops created by Coulomb explosions, which evolve near the Rayleigh limit, and, for some reason, do not reach the field-evaporation regime.

The central mode II is the only one surviving the suppression of Coulomb explosions. It must hence be associated with residues from relatively large drops evolving in the ion evaporation regime, whose charge departs increasingly from the Rayleigh limit as their diameters decrease. Since these drops typically have diameters larger than 10 nm, the d_0 correction on the Z/E ratio is small, and their mobility Z is nearly proportional to E. Furthermore, their curvature is modest, so that, when based on this mode, the interpretation of [31] of an approximately constant surface electric field E is essentially correct (notice the narrowness of the $S = 0$ peak in Fig. 9). Taking $Z^{-1} = 2.31$ Vs/cm^2 (Figs. 2, 8), we find $E = 1.19$ V/nm, quite close to the earlier determination based on the suppression of Coulomb explosions. The more detailed and precise work of de Juan [55] has shown that this surface field increases slightly at decreasing drop diameters for mode II, and has also captured the sharp transition between modes I and II.

The most mobile mode III is studied here for the first time. It contains a fair fraction of the spray residues (being readily detected with a CNC), but carries a small portion of the spray charge (being hard to investigate with an electrometer). It disappears in the absence of Coulomb explosions because there is then no mechanism to create such small entities. The lower size end of this mode contains doubly (perhaps also singly) charged clusters with as few as 6 tetraheptyl groups (cluster diameters below 1.9 nm and perhaps smaller), attesting to the tremendous atomizing power of Coulomb explosions. This mode is also characterized by a charge limited by ion evaporation, but has no longer an approximately constant electric field. There are two reasons for this. First, the d_0 correction in (1) is not negligible [24], and leads for a fixed E to smaller mobilities than in the larger particles of mode II. Second, the effect of curvature on activation energy is not negligible either, so that E ceases to be fixed. The observation that this mode has higher mobilities than mode II in spite of the reduced Z/E ratio implies that the surface fields increase with decreasing diameter.

6. Conclusions

By turning off the mechanism of Coulomb explosions in highly conducting solutions at suffi-

ciently small liquid flow rates, we have identified the different roles played by the charged residue and the ion evaporation mechanism in electrospray ionization of tetraheptyl ammonium bromide (A^+B^-) dissolved in formamide. Coulomb fissions are responsible for the production of all multiply charged clusters $(A^+)_z(A^+B^-)_n$ observed (except the very largest), incuding ions at least as small as $(A^+)_2(A^+B^-)_4$. Ion evaporation produces only singly charged clusters ($z=1$), with n from 0 to at most 6. But it marks profoundly the whole process of multiply charged cluster formation, fixing the maximum and minimum level of aggregation $n_{\max}(z)$ and $n_{\min}(z)$ present at a given z. A qualitative prediction from this picture is that $n_{\max}(z) \sim n_{\min}(z+1)$. It is confirmed experimentally in the striking modulated structure of the mobility spectra of partially neutralized clusters (where z is reduced to unity for all sizes). Each modulation spans a finite mobility band and contains almost exclusively clusters with one initial z. The various bands are ordered according to this initial z, and are exaclty adjacent to each other.

The key role played by ion evaporation from the drops is confirmed further by the facts that (i) Coulomb fissions are suppressed when the initial electrospray drops have surface electric fields E above 1 V/nm. (ii) Clusters are charged well below the Rayleigh limit (37% for $z=2$). (iii) A drastic simplification of the mobility spectra is seen when the spray drops reach a critical field.

As pointed out before by a diversity of authors, neither the CRM nor the IEM can account for all the observations made. But it does not follow that either of these mechanisms can be discarded. In fact, the two models need to be invoked separately to explain different aspects of the total phenomenology observed. Both mechanisms act together, each doing part of the ionization job.

The experimental curves $n_{\max}(z)$ and $n_{\min}(z)$ carry key information on the ion evaporation kinetics. They determine the solvation energy of the ejected ions as a function of the radius and charge of the parent drops, $\Delta = \Delta(R, z)$. The picture of [31] needs to be extended for the smallest drops to incorporate curvature effects, as confirmed theoretically in the Appendix A.

Acknowledgements

We are indebted to Drs. I.G. Loscertales, L. de Juan, J.B. Fenn and M. Labowsky for many enlightening discussions on this complex subject. The measurements described would not have been possible without the work of Drs. K. Okuyama and T. Seto on the PSM, Mr. Thilo Eichler's on the DMA and Dr. S. Kaufman's [46–48] on the neutralization technique. This research has been supported by the U.S. National Science Foundation grant CTS-9319151.

Appendix A. Modeling the effect of curvature on ion solvation energy

Let us retain the simplification of a very high dielectric constant, but relax the neglect of surface curvature. For a spherical drop of radius R the polarization potential then degenerates into the image potential on a point elementary charge in the vicinity of a conducting sphere, which may be written in terms of the distance r to the center of the drop as [63]:

$$W = C_1 + \frac{e^2}{4\pi\varepsilon_0 R}\left\{z\left(\frac{1}{x}-1\right) - \frac{1}{2x^2(x^2-1)}\right\};$$
$$x = r/R; \quad (x-1)R \gg 1\,\text{Å} \tag{A1}$$

where, again, (A1) holds when $(x-1)R \gg 1$ Å, while the constant C_1 is chosen such that the origin of energies is at the liquid surface. The term z/x is the Coulombic repulsion due to the z charges remaining in the drop after the ejection of the ion. In the vicinity of the surface (A1) must be replaced by

$$W = \phi_0(x) + \frac{e^2}{4\pi\varepsilon_0 R} z\left(\frac{1}{x}-1\right) \tag{A2}$$

with $\phi_0(1) = 0$ and

$$\phi_0(x) \to C_1 - \frac{e^2}{8\pi\varepsilon_0 R}\,\frac{1}{x^2(x^2-1)}; \quad y \gg 1\,\text{Å} \tag{A3}$$

The position, x^*, of the maximum of W is found by the condition that the derivative of (A1) with respect to x vanishes, which leads to the following relation between z and x^*:

$$z(x^*)\frac{x^{*3}}{(x^{*2}-1)^2} - \frac{1}{x^*} \tag{A4}$$

The inverse relation $x^*(z)$ is readily determined numerically, and shown in Table 4. Its asymptote for large z is

$$x^*(z) = 1 + \frac{1}{2}z^{-1/2} + \frac{1}{4}z^{-1} - \frac{9}{64}z^{-3/2} + \mathrm{O}(1/z^2); \quad z \gg 1 \tag{A5}$$

The barrier height is:

$$\Delta = W(x^*) = \mathrm{C}_1 + \frac{e^2}{4\pi\varepsilon_0 R}F(z) \tag{A6}$$

where the function $F(z)$ is defined parametrically in terms of z by means of $x^*(z)$ as

$$F(z) = \left\{ z\left[\frac{1}{x} - 1\right] - \frac{1}{2x^2(x^2-1)} \right\}_{x=x^*(z)} \tag{A7}$$

as shown also in Table 4 for z from 1 to 10. Its asymptotic behavior at large z is

$$F(z) = z^{1/2} - 7/8 + \mathrm{O}(z^{-1/2}); \quad z \gg 1 \tag{A8}$$

Now one is faced with the task of determining the constant C_1. As before for C, C_1 is the energy required to bring the ion from the liquid into infinity when $z = 0$. However, unlike C, we cannot assure that $\mathrm{C}_1 = \Delta G^0_{\mathrm{S}}$ because this solvation energy could well depend on the drop radius. The importance of this curvature effect may be seen in the case of a hypothetical ion whose radius is small, in the range of 1 Å. In this case, the far field attractive potential applies down to relatively near the wall, where (A3) can be expanded in powers of the distance to the wall, $y = R(x-1)$, leading to

$$\phi_0(x) \to \mathrm{C}_1 - \frac{e^2}{16\pi\varepsilon_0 R}\left\{\frac{-R}{y} - \frac{5}{2} + \cdots\right\} \tag{A9}$$

Simultaneously, the effect of curvature on the near-wall attraction must be very small at such small distances from the surface. This means that $\phi_0(x)$ must be practically identical to $\phi(x)$ in this near-wall region. Hence, identifying (A9) and (6c) we see that they do in fact coincide except for a constant, and they become identical when

$$\mathrm{C}_1 = \Delta G^0_{\mathrm{S}} - \frac{5e^2}{32\pi\varepsilon_0 R} \tag{A10}$$

The conclusion is that the solvation energy is indeed decreased by curvature by the amount shown in equation (A10). Physically, this reasoning amounts to saying that the near-wall portion of the attractive potential is unchanged by the curvature, because R is much larger than typical interatomic potential forces. Hence, all the changes in the interaction happen in the outer region, where curvature is no longer negligible. But the outer field is well known with and without curvature. One can then compare both to see how they differ. Setting their zero energy point to the same value at infinity, one then sees (via Laurent expansion near $y = 0$) that their value near the wall differs by the quantity $5e^2/(32\pi\epsilon_0 R)$, as in (A10).

Mathematically, this reasoning is of course typical of problems with two very different length scales, where the inner behavior of a function has to be matched with its outer behavior. When the disparity of scales is sufficient, one boldly states that the limit of the outer function as y tends to zero is equal to the limit of the inner function as y tends to infinity. This asymptotic matching procedure is exactly the one followed in identifying (A9) and (6c). It probably fails when there is no large scale disparity, such as in the case of our rather bulky tetraheptyl ammonium ions, but it may hold for the case of solvated ions of alkali metals. In any case, what these model examples suggest is that the activation energy Δ has the form

$$\Delta = \Delta G^0_{\mathrm{S}} - \frac{e^2}{4\pi\varepsilon_0 R}[F(z) + \alpha] \tag{A11}$$

where the dimensionless solvation energy shift α takes the value 5/8 for a very small ion. For our experiments with tetraheptyl ammonium bromide, α is probably not null, but does not necessarily take the value 5/8 corresponding to small ions.

Notice finally in (A11) that the α term represents a correction due strictly to the curvature and not the charge, while the $F(z)$ term due to the net charge depends on curvature in a well established form. The main ambiguity is therefore, on the α term, where one does not in principle know if α itself is a function of R. On the other hand, the curvature correction $\alpha\epsilon^2/(4\pi\epsilon_0 R)$ is directly proportional to the curvature $1/R$. Hence, even in problems in which the model leading to (A11) may not apply, this result may still be valid with a certain value of α as the first correction in a small curvature approximation. Of course, this would require that Δ be an analytic function in $1/R$, whereby a Taylor expansion in powers of $1/R$ would exist.

References

[1] S.F. Wong, C.K. Meng, J.B. Fenn, Multiple charging in electrospray ionization of poly(ethylene glycols), J. Phys. Chem. 92 (1988) 546–550.

[2] J.B. Fenn, M. Mann, C.K. Meng, S.K. Wong, C. Whitehouse, Science 246 (1989) 64–71.

[3] J.B. Fenn, M. Mann, C.K. Meng, S.K. Wong, Electrospray ionization, principles and practice, Mass spectrom. Rev. 9 (1990) 37–70.

[4] R.D. Smith, J.A. Loo, R.R.O. Loo, M. Busman, H.R. Udseth, Principles and practice of electrospray ionization — mass-spectrometry for large polypeptides and proteins, Mass Spectrom. Rev. 10 (1991) 359–451.

[5] A.L. Burlingame, R.K. Boyd, S. Gaskell, Mass spectrometry Review, Anal. Chem. 70 (1998) 647R–716R.

[6] C.K, Meng, Multiple and fractional charging of solute molecules in electrospray ionization, Ph.D. Thesis, Yale University, 1988.

[7] C.K. Meng, J.B. Fenn, Formation of charged clusters during electrospray ionization of organic solute species, Organic Mass Spectrom. 26 (1991) 542–549.

[8] J.V. Iribarne, B.A. Thomson, On the evaporation of small ions from charged droplets, J. Chem. Phys. 64 (1976) 2287–2294.

[9] B.A. Thomson, J.V. Iribarne, Field induced ion evaporation from liquid surfaces at atmospheric pressure, J. Chem. Phys. 71 (1979) 4451–4463.

[10] B.A. Thomson, J.V. Iribarne, P.J. Dziedzic, Liquid ion evaporation/mass spectrometry for the detection of polar labile molecules, Anal. Chem. 54 (1982) 2219–2224.

[11] B.A. Thomson, Atmospheric pressure ionization and liquid chromatography mass spectrometry. Together at last, J. Am. Soc. Mass Spectrom. 9 (1998) 187–193.

[12] J.F. Anacleto, S. Pleasance, R.K. Boyd, Calibration of ion spray mass-spectra using cluster ions, Organic Mass Spectrom. 27 (1992) 660–666.

[13] C.E.C.A. Hop, Generation of high molecular weight cluster ions by electrospray ionization; implications for mass calibration, J. Mass Spectrom. 31 (1996) 1314–1316.

[14] C.E.C.A. Hop, D.A. Saulys, D.F. Gaines, Electrospray mass-spectrometry of borane salts — the electrospray needle as an electrochemical-cell, J. Am. Soc. Mass Spectrom. 6 (1995) 860–865.

[15] C.E.C.A. Hop, D.A. Saulys, D.F. Gaines, Electrospray mass-spectrometry of borane salts — observation of high-molecular-weight ion clusters, Inorg. Chem. 34 (1995) 1977–1978.

[16] G.D. Wang, R.B. Cole, Solvation energy and gas-phase stability influences on alkali metal cluster ion formation in electrospray ionization mass spectrometry, Anal. Chem. 70 (1998) 873–881.

[17] B.E. Winger, K.J. Lightwahl, R.R.O. Loo, H.R. Udseth, R.D. Smith, Observation and implications of high mass-to-charge ratio ions from electrospray-ionization mass-spectrometry, J. Am. Soc. Mass Spectrom. 4 (1993) 536–545.

[18] S.L. Zhou, M. Hamburger, Formation of sodium cluster ions in electrospray mass spectrometry, Rapid communications in mass spectrometry 10 (1996) 797–800.

[19] D.R. Zook, A.P. Bruins, On cluster ions, ion transmission and linear dynamic range limitations in electrospray (ionspray) mass spectrometry, Int. J. Mass Spectrom. Ion Processes 162 (1997) 129–147.

[20] P. Kebarle, M. Peschke, On the mechanism by which the charged droplets produced by electrospray lead to gas phase ions. Anal. Chim. Acta, this issue.

[21] J. Rosell, I.G. Loscertales, D. Bingham, J. Fernández de la Mora, Sizing nanoparticles and ions with a short differential mobility analyzer, J. Aerosol Sci. 27 (1996) 695.

[22] L. de Juan, J. Fernández de la Mora, Size analysis af nanoparticles and ions: running a Vienna DMA of near optimal length at Reynolds numbers up to 5000, J. Aerosol Sci. 29 (1998) 617–626.

[23] T. Eichler, Senior Graduation Thesis presented to Fachhochscule Offenburg, Germany, 1997.

[24] H. Tammet, Size and mobility of nanometer particles, clusters and ions, J. Aerosol Sci. 26 (1995) 459–475.

[25] J. Fernández de la Mora, L. de Juan, A. Schmidt-Ott, On the relation between size and mobility in the nanometer range, submitted for publication to J. Aerosol Sci., 1998.

[26] J. Fernández de la Mora, L. de Juan, T. Eichler, J. Rosell, Differential mobility analysis of molecular ions and nanometer particles, Trends Anal. Chem. 17 (1998) 328–339.

[27] K. Okuyama, Y. Kousaka, T. Motouchi, Aerosol Sci. Technol. 3 (1984) 353.

[28] T. Seto, K. Okuyama, J. Fernández de la Mora, Condensation of supersaturated vapors on monovalent and divalent ions of varying size, J. Chem. Phys. 107 (1997) 1576–1585.

[29] M. Gamero-Castaño, J. Fernández de la Mora, A condensation nucleus counter (CNC) sensitive to singly charged sub-nanometer particles, submitted for publication to J. Aerosol Sci., March, 1999.

[30] M. Gamero-Castaño, The transfer of ions and charged nanoparticles from solution to the gas phase in electrosprays. Ph.D. Thesis, Yale University, 1999.

[31] I.G. Loscertales, J. Fernández de la Mora, Experiments on the kinetics of field evaporation of small ions from droplets, J. Chem. Phys. 103 (1995) 5041–5060.

[32] M. Gamero-Castaño, J. Fernández de la Mora, Stopping potential investigation of Taylor cone-jets of electrolytes in vacuo, submitted to Physics of Fluids, 1999.

[33] M. Gamero-Castaño, J. Fernández de la Mora, Direct measurement of ion evaporation kinetics from Taylor cone-jets, submitted to J. Chem. Phys., April, 1999.

[34] R. Guevremont, K.W.M. Siu, J.Y. Wang, L.Y. Ding, Combined ion mobility time-of-flight mass spectrometry study of electrospray-generated ions, Anal. Chem. 69 (1997) 3959–3965.

[35] M. Dole, L.L. Mach, R.L. Hines, R.C. Mobley, L.P. Ferguson, M.B. Alice, J. Chem. Phys. 49 (1968) 2240.

[36] L. Rayleight, On the equilibrium of conducting masses charged with electricity, Phil. Mag. 14 (1882) 184–186.

[37] L. Rayleight, The Theory of Sound, Dover, New York, 1945, sect. 364, p. 374.

[38] J.M.H. Peters, Rayleigh's electrified water drops, Eur. J. Phys. 1 (1980) 143–146.3.

[39] J.B. Fenn, J. Rosell, T. Nohmi, S. Shen, F.J. Banks, Jr., Electrospray ion formation: desorption versus desertion, in: P. Snyder (Ed.), Biochemical and Biotechnological Applications of Electrospray Ionization Mass Spectrometry, ACS Symposium Series 619, 1996, pp. 60–80.
[40] J. Fernández de la Mora, On the outcome of the Coulomb fission of a charged isolated drop, J. Colloid Interface Sci. 178 (1996) 209–218.
[41] E.J. Davis, M.A. Bridges, The Rayleigh limit of charge revisited: light scattering from exploding droplets, J. Aerosol Sci. 25 (1994) 1179–1199.
[42] L. de Juan, J. Fernández de la Mora, J. Colloid Interface Sci. 186 (1997) 280.
[43] J. Rosell, Size characterization in electrosprays of submicron droplets, Ph.D. Thesis, Yale University, New Haven, CT, USA, 1994.
[44] T. Nohmi, J.B. Fenn, J. Am. Chem. Soc. 114 (1992) 3241, 3246.
[45] L. de Juan, J. Fernández de la Mora, On-line sizing of colloidal nanoparticles via electrospray and aerosol techniques, in: G.M. Chow, K. Gonsalves (Eds.), Nanotechnology, Molecularly Designed Materials, ACS symposium series 622, ACS, Washington, DC, 1996, pp. 20–41.
[46] S.L. Kaufman, J.W. Skogen, F.D. Dorman, F. Zarrin, L.C. Lewis, Macromolecule analysis based on electrophoretic mobility in air: globular proteins, Anal. Chem. 68 (1996) 1895–1904.
[47] S. Mouradian, J.W. Skogen, F.D. Dorman, F. Zarrin, S.L. Kaufman, L.M. Smith, DNA analysis using an electrospray scanning mobility particle sizer, Anal. Chem. 69 (1997) 919–925.
[48] S.L. Kaufman, Analysis of biomolecules using electrospray and nanoparticle methods: the gas-phase electrophoretic mobility molecular analyzer (GEMMA), J. Aerosol Sci. 29 (1998) 537–552.
[49] J. Fernández de la Mora, Electrospray ionization of multiply charged globular proteins and dendrimers proceeds via Dole's charged residue mechanism, Anal. Chim. Acta, this issue.
[50] A. Gomez, K. Tang, Charge and fission of droplets in electrostatic sprays, Phys. Fluids 6 (1994) 404–414.
[51] F.W. Röllgen, E. Bramer-Weger, L. Bütfering, Field ion emission from liquid solutions: ion evaporation against electrohydrodynamic disintegration, J. Physique 48 (1987) C6 253-256.
[52] G. Schmelzeisen-Redeker, L. Bütfering, F.W. Röllgen, Int. J. Mass Spectrom. Ion Proc. 90 (1989) 139–150.
[53] F.M. Röllgen, H. Nehring, U. Giessmann, Mechanisms of field induced desolvation of ions from liquids, in: A. Hedin, B.U.R. Sundqvist, A. Beninghoven (Eds.), Ion Formation From Organic Solids, Wiley, Chichester, 1989, pp. 155–160.
[54] M. Labowski, Discrete charge distributions in dielectric drops, J. Colloid Interface Sci. 206 (1998) 18–28.
[55] L. de Juan, Characterization and generation of charged aerosols by tandem spectrometry and electrospray source, Ph.D. Thesis, Yale University, 1998.
[56] V. Katta, A.L. Rockwood, M.L. Vestal, Int. J. Mass Spectrom. Ion Proc. 103 (1991) 129–148.
[57] J.B. Fenn, J. Rosell, C.K. Meng, Electrospray ionization, how much pull does an ion need to escape its droplet prison?, J. Am. Soc. Mass Spectrom. 8 (1997) 1147–1157.
[58] J. Rosell, J. Fernández de la Mora, 0.3–4μm in diameter from electrified cone-jets of highly conducting viscous liquids, J. Aerosol Sci. 25 (1994) 1093–1119.
[59] J. Fernández de la Mora, I.G. Loscertales, The current transmitted through an electrified conical meniscus, J. Fluid Mech. 260 (1994) 155–184.
[60] D.R. Chen, D.Y.H. Pui, K. Kaufman, S. Kaufman, Electrosprays of conducting liquids for monodisperse aerosol generation in the 4 nm to 1.8 μm diameter range, J. Aerosol Sci. 26 (1995) 963–977.
[61] D.R. Chen, D.Y.H. Pui, Aerosol Sci. Technol. 27 (1997) 367–380.
[62] A.M. Gañán-Calvo, J. Dávila, A. Barrero, Current and droplet size in the electrospraying of liquids. Scaling laws, J Aerosol Sci. 28 (1997) 249–275.
[63] L.D. Landau, E.M. Lifshitz, Electrodynamics of continuous media, chap. 1, sect. 3.